Available online at www.sciencedirect.com

SciVerse ScienceDirect

Geochimica et Cosmochimica Acta 106 (2013) 463–489

Geochimica et Cosmochimica Acta

www.elsevier.com/locate/gca

Murchison presolar carbon grains of different density fractions: A Raman spectroscopic perspective

B. Wopenka [a,*], Y.C. Xu [b,1], E. Zinner [b], S. Amari [b]

[a] Department of Earth and Planetary Sciences, One Brookings Drive, Washington University, St. Louis, MO 63130-4899, USA
[b] Laboratory for Space Sciences and the Physics Department, Washington University, St. Louis, MO 63130-4899, USA

Received 27 September 2012; accepted in revised form 12 December 2012; available online 5 January 2013

Abstract

Raman analyses are reported of μm-sized areas of 103 individual carbonaceous presolar grains ("graphite grains") from three different density fractions of the Murchison meteorite. Few of the grains (2 or 3 of each density fraction) have Raman spectra typical for non-crystalline sp^2-bonded carbon (i.e., "organic carbon") with extremely wide 1st-order and no (or very subdued) 2nd-order peaks, similar to the ones found for terrestrial kerogens. Based on depth profiles of isotopic ratios measured with the NanoSIMS, it is unlikely that such kerogen-type Raman signatures are caused by contamination of the presolar grains with insoluble organic material from the Murchison matrix that stuck to the surfaces of the grains. Rather, the kerogen-type grains are considered to be a new type of presolar carbon grains, which are made up of organic (PAH-like) sp^2-bonded carbon. However, most of the other studied presolar carbon grains (95 of 103) have spectra with very narrow 1st-order peaks (called *D* and *G* peaks) and very strong 2nd-order peaks typical for inorganic sp^2-bonded carbon. Based on their D/G intensity ratios, those grains were grouped into the following Raman types: (fairly well ordered) "graphite" ($D/G < 0.5$), "disordered graphite" ($0.5 < D/G < 1.1$), "glassy carbon" ($D/G > 1.1$), and "unusual sp^2-bonded graphitic carbon" (with extremely intense 2nd-order peaks relative to the 1st-order peaks). Grains from the low-density fraction KFA1 (2.05–2.10 g/cm^3) have predominantly "cauliflower" morphology and Raman spectra characteristic of either very disordered graphite or "glassy carbon" (i.e., the latter is amorphous from the Raman spectroscopic perspective), whereas most grains from the high-density fraction KFC1 (2.15–2.20 g/cm^3) have "onion" morphology and Raman spectra characteristic of well-crystalline graphite. The KFB1 grains with intermediate density (2.10–2.15 g/cm^3) are mixed, both in terms of their morphology and their Raman spectra but are closer to KFC1 than to KFA1 grains. The correlation of the Raman results with both morphology and isotopic data show that presolar sp^2-bonded carbon grains from different stellar sources differ in their crystalline structure. Grains that dominate the high density fractions and whose isotopic ratios indicate an origin in AGB stars consist of well crystallized graphite, whereas grains that dominate the low-density fraction and whose isotopic ratios indicate a supernova origin consist of very disordered graphite or even of amorphous "glassy carbon".

1. INTRODUCTION

1.1. Nomenclature of presolar carbon grains

So-called "graphite grains" (Amari et al., 1990) are one of the many different types of presolar grains found in primitive meteorites (Zinner, 2007). Historically, the term "graphite" was used for all carbonaceous presolar grains that were isolated from meteorites with acidic digestive procedures, and that were known not to be diamond and silicon carbide (e.g., Amari et al., 1990, 1995a; Zinner, 2007). We know, however, that not all grains that are

* Corresponding author. Tel.: +1 314 935 4771.
E-mail addresses: bwopenka@levee.wustl.edu (B. Wopenka), ekz@wustl.edu (E. Zinner).
[1] Present address: Chinese Academy of Sciences, Guiyang 550002, China.

0016-7037/$ - see front matter © 2013 Elsevier Ltd. All rights reserved.
http://dx.doi.org/10.1016/j.gca.2012.12.022

referred to as "graphite grains" by the astrophysics and cosmochemistry communities have the structure of well crystallized sp^2-bonded carbon that is known as graphite to mineralogists. Materials that are not confirmed to have a well-defined crystallographic order, however, should strictly speaking not be called "graphite". Indeed, detailed TEM studies (Bernatowicz et al., 1991, 1996; Croat et al., 2003, 2008) have documented that many of the presolar grains are not well-crystalline graphite consisting of flat stacked layers of sp^2-bonded carbon, but rather that they consist of poorly-crystalline or nanocrystalline carbon. Bernatowicz et al. (1991) have documented more than 20 years ago that many of the presolar socalled "graphite" grains have short, curved and discontinuous layers that lack long-range continuity. It also was noted that the densities of some of the "graphite" fractions of Murchison and Orgueil are substantially lower than the ones listed for well-crystalline graphite (2.09–2.23 g/cm^3). Such low densities were found especially for grains with so-called "cauliflower" morphology (Hoppe et al., 1995). Previous Raman studies (Jadhav et al., 2010; Wopenka et al., 2011a,b; Zinner et al., 1995), as well as our present study also show that not all presolar sp^2-bonded carbon grains deserve to be called "graphite", as least from the Raman spectroscopic perspective. Indeed, based on Raman analysis, some of the presolar carbon grains have to be considered amorphous, and are either inorganic so-called "glassy carbon", or even consist of hydrogenated aromatic macromolecular (i.e., kerogen-like or PAH-like) organic carbon.

In spite of all these findings obtained with different analytical techniques, it continued to be the tradition to refer to all sp^2-bonded carbon grains, even the ones with curved, discontinuous layers and no long-range crystallographic order, as "graphite". From the mineralogists' perspective this nomenclature is incorrect, because graphite (and any other mineral) is defined by both its chemistry and its long-range crystallographic order. But because of this long-standing tradition of nomenclature used by the presolar grain community, in the present paper we also will continue to use the generic term "graphite grains" to refer to the sp^2-bonded presolar carbon grains. However, we alert the reader to the fact that "sp^2-bonded carbon grains" (a nomenclature that we also will use in the present paper) would be a more appropriate term for many of these grains.

1.2. Presolar graphite: a short overview of the state of knowledge

Most presolar studies in the past were performed on SiC grains (Zinner, 2007; Hynes and Gyngard, 2009), but data also have been obtained on >1000 individual presolar graphite grains (see Hynes and Gyngard, 2009 for isotopic data). The separation procedures for graphitic grains are more complicated than those for SiC grains because the so-called insoluble organic matter (IOM), i.e., the abundant organic (i.e., amorphous) carbonaceous matrix material (Amari et al., 1994) has to be removed without destroying the graphite. Thus, the necessary procedures consist of dissolution of silicates, removal of sulfur, followed by a mild oxidation to remove (most of) the IOM. The resulting residue ("acid residue") then can be separated into various density fractions. Graphite grains so far have been isolated from two meteorites: CM2 Murchison and CI1 Orgueil, and separates of different densities (ranging from 1.6–2.05 g/cm^3 to 2.15–2.20 g/cm^3 for the Murchison K-series (Amari et al., 1994), and from 1.59–1.67 g/cm^3 to 2.16–2.30 g/cm^3 for the Orgueil OR1 series (Jadhav et al., 2006) have been available for study. Almost all of the information we have about presolar graphite grains comes from these two separations.

Previous studies of presolar graphite grains (see chapter on graphite in Zinner, 2007) include noble gas measurements of four Murchison density fractions from the K-series, on "bulk" samples and on single grains (Nichols et al., 1995; Amari et al., 1995a; Heck et al., 2009; Meier et al., 2012). Isotopic analyses by secondary ion mass spectrometry (SIMS) have been performed on a large number of grains from Murchison and Orgueil (Hynes and Gyngard, 2009). In addition, isotopic measurements have been made by resonance ionization mass spectrometry (RIMS) on individual grains from Murchison (Nicolussi et al., 1998) and Orgueil (Jadhav et al., 2012). Detailed transmission electron microscope (TEM) studies probed the internal structure and chemistry of presolar graphite grains and of subgrains therein (Bernatowicz et al., 1991, 1996; Croat et al., 2003, 2005, 2010).

Isotopic studies indicate that low-density grains generally come from Type II supernovae (Amari et al., 1995b, 1996; Nittler et al., 1996; Travaglio et al., 1999; Stadermann et al., 2005; Zinner et al., 2006a) and that high-density grains come from AGB stars of low metallicity (Amari et al., 1995a; Croat et al., 2005; Jadhav et al., 2006, 2008; Zinner et al., 2006a). Low-density grains typically have low $^{14}N/^{15}N$, $^{16}O/^{18}O$, $^{29}Si/^{28}Si$, and $^{30}Si/^{28}Si$ ratios as well as high $^{26}Al/^{27}Al$ ratios. The initial presence of the short-lived ($\tau_{1/2} = 730{,}000$ years) radioisotope ^{26}Al is inferred from large excesses in the daughter isotope ^{26}Mg. Some grains also have large ^{44}Ca excesses, interpreted to come from the decay of short-lived ^{44}Ti ($\tau_{1/2} = 60$ years). All these isotopic signatures can, in principle, be explained by nucleosynthesis in massive (>10 $M_\odot$) stars that explode as core-collapse supernovae. In particular, ^{28}Si and ^{44}Ti can be produced only in supernovae (Timmes et al., 1996). High-density grains have higher $^{12}C/^{13}C$ ratios than low-density grains. Some of the high-density grains have excesses in ^{29}Si and ^{30}Si with $\delta^{29}Si/\ \delta^{30}Si$ values much smaller than 1; this signature is consistent with theoretical predictions for AGB stars of low metallicity (Zinner et al., 2006b). In contrast, few low-density grains have excesses in ^{29}Si and ^{30}Si with $\delta^{29}Si/\delta^{30}Si \sim 1$. Low-metallicity AGB stars are predicted to have higher $^{12}C/^{13}C$ ratios than AGB stars of solar metallicity. High $^{12}C/^{13}C$ ratios imply high C/O ratios, which can explain the preferential condensation of graphite over SiC in the stellar winds from low-metallicity stars. In AGB stars, ^{12}C produced in the He intershell is mixed to the surface during third-dredge-up episodes, increasing both the C/O and $^{12}C/^{13}C$ ratio (Zinner et al., 2006a). TEM studies of TiC subgrains in high-density grains found large overabundances of the heavy elements

Zr, Mo, and Ru in these subgrains (Croat et al., 2005), and thus confirm their AGB origin. These elements are produced by the s-process in AGB stars and are predicted to be abundant in the atmosphere of such stars. In contrast, TiC subgrains in low-density grains with an implied supernova origin do not have such overabundances of heavy elements. In addition to grains from supernovae and AGB stars, some high-density Orgueil grains with extreme Ca and Ti isotopic anomalies have been proposed to have originated from born-again AGB stars (Jadhav et al., 2008).

1.3. Previous Raman studies of presolar carbon grains

We have already reported Raman measurements for a different Murchison separate (Zinner et al., 1995, see discussion below), as well as for the Orgueil high-density separate OR1f (Jadhav et al., 2010; Wopenka et al., 2011b) and the Orgueil low-density separate OR1d (Wopenka et al., 2011a). Our previous Raman study of Murchison grains (Zinner et al., 1995) was performed on separate LFC1 from the L-series (Amari et al., 1994). These early Raman measurements suffered from several shortcomings. First, they were not made on grains from separates of different known densities such as those from the K-series, but rather on grains with a density range from 1.75 to 2.2 g/cm^3. This large density range of the L-series grains encompasses the three density fractions KFA1, KFB1, and KFC1 from the Murchison K-series for which we report data in the present paper. Second, the Raman analyses were made with a first-generation Raman spectrometer, a single-channel Jobin–Yvon RAMANOR U-1000 laser Raman microprobe. Even though this was a highly sensitive confocal instrument with excellent wavenumber accuracy, it had one disadvantage compared to today's Raman instrumentation: the wavelength range was scanned sequentially, and thus it could take up to 8 h to obtain a full Raman spectrum on a micrometer-sized spot. As a consequence, the sample was exposed for long periods (up to 8 h per spectrum) to laser-induced heating, and in addition, the laser power used was much higher than what is recognized today to be the appropriate excitation power for the analysis of sp^2-bonded carbon. Therefore, we suspect that some Raman spectra of the 1995 study that had indicated fairly well-crystalline graphite might not have reflected necessarily the original crystallinity of the grains, but rather could have been the result of graphitization by heating during the long time that was needed for analysis. Third, the Raman spectra for the 1995 study were obtained on grains that had previously been analyzed in the ion microprobe. Today, we know that the sputtering process in the ion probe affects the structure of graphite grains (see below), and that Raman studies need to be performed on grains that have not yet suffered beam damage during SIMS analysis.

1.4. The present Raman study

Because of the shortcomings of the Zinner et al. (1995) study, in the present work we re-visit after an almost 20 year lull the Raman analyses of presolar Murchison graphite grains. We now have more knowledge and experience about presolar grains in general, more experience with the Raman analysis of heat-sensitive sp^2-bonded carbonaceous materials, and better instruments and analytical protocols. We analyzed a total of 103 individual density-separated presolar carbon grains from the Murchison fractions KFA1, KFB1, and KFC1. We investigated (1) whether the Raman signature of the grains provides any information with respect to the crystallinity or structural order of the sp^2-bonded carbon, (2) whether grains of different density have different Raman spectra, and (3) whether there exists any correlation between the Raman spectral parameters and the isotopic composition of individual grains. Raman analyses were followed by isotopic analyses in the NanoSIMS. Preliminary results of this Raman study have been reported by Wopenka et al. (2012).

2. SAMPLES AND EXPERIMENTAL TECHNIQUES

2.1. Isolation of presolar graphite grains

A detailed description of the separation procedure of the Murchison K-series, performed at the University of Chicago, is given by Amari et al. (1994). The essential steps in this procedure were the dissolution of silicates by alternating treatment with HCl-HF and HCl, removal of sulfur with KOH, oxidation with H_2O_2 and $Na_2Cr_2O_7$–H_2SO_4, colloidal extraction of diamonds, and finally density and size separations. An essential step in the isolation of graphite grains was the use of dichromate ($Na_2Cr_2O_7$) in order to gently oxidize (and thus remove) the dominant organic insoluble carbonaceous material (IOM), while at the same time not to oxidize (and thus preserve) the inorganic insoluble carbonaceous material (graphite grains). This procedure of selective oxidation was very successful, and the resulting density fractions of graphite, KE3 (1.6–2.0 g/cm^3), KFA1 (2.05–2.10 g/cm^3), KFB1 (2.10–2.15 g/cm^3), and KFC1 (2.15–2.20 g/cm^3) were essentially free of IOM contamination. [As a note on the side, the latter was unfortunately not the case for the same kind of chemical isolation procedures of presolar graphite grains from the Orgueil meteorite, during which not all of the organic IOM was successfully oxidized (Jadhav et al., 2006, 2013), and thus the surface of many of the Orgueil presolar graphite grains are contaminated with IOM (or "organic crud" as we call it at Washington University)].

2.2. Sample preparation and sequence of analytical techniques used

Graphite grains from the three selected density fractions were deposited on gold foil from a water–propanol suspension. Various isotopic standards for the NanoSIMS isotopic analysis were also mounted on the gold foil. The individual grains were first photo-documented in the scanning electron microscope (SEM) to determine their position on the sample holder and to obtain their sizes. Grains larger than 3 μm in diameter were selected for analysis. Of these grains, secondary electron images were obtained in an Auger nanoprobe to determine their surface morphology. (Note that in addition of being equipped with an Auger

electron spectrometer, the Auger nanoprobe also can detect secondary electrons; due to the instrument's field emission electron gun those images result in a higher spatial resolution compared to the ones that can be obtained with our conventional SEM.) Maps of the locations of the selected grains on the Au mounts were obtained in an optical microscope for Raman analysis. Based on their appearance in SEM pictures, the grains were grouped into "cauliflowers", "onions" and "cauliflower–onions" (i.e., the ones with mixed, unclear and/or ambiguous appearances). The "cauliflower–onions" correspond roughly to what Hoppe et al. (1995) called "cauliflower-type grains with fine surface texture" (CF-f), and what are referred to as "caulionions" in Xu et al. (2012). Subsequently, Raman spectra of 103 individual presolar grains from the KFA1, KFB1, and KFC1 density fractions were acquired. Only after completion of the Raman study were the grains studied for their isotopic composition in the NanoSIMS. This sequence of analyses (first SEM, then Raman, then NanoSIMS) is important because NanoSIMS analysis is destructive; it not only sputters the sample away, but it also destroys and/or changes the crystallographic structure of the remaining sp^2-bonded materials (e.g., Lucchese et al., 2010). The latter can be seen by comparing the Raman spectra of a given sp^2-bonded carbonaceous sample before and after SIMS analysis (Fig. 1). Obviously, because of this sequence of analyses, the presolar nature of individual grains could only be confirmed after the Raman analyses were finished.

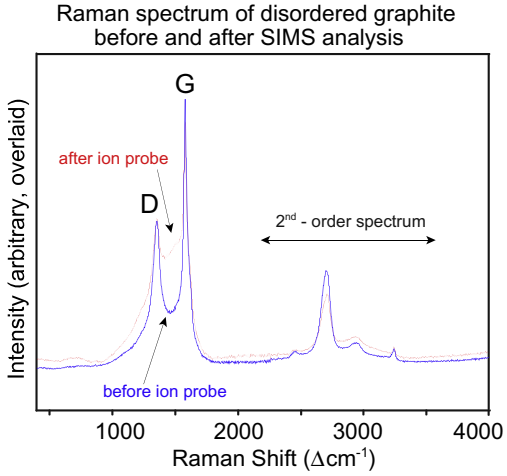

Fig. 1. Effect of ion bombardment on the Raman spectrum is shown by comparing the Raman spectra of disordered graphite before and after NanoSIMS analysis. The sample is the terrestrial disordered graphite that is used in the Washington University SIMS laboratories as isotopic standard to determine $^{12}C/^{13}C$ ratios. The implantation of ions during SIMS analysis obviously affects the sp^2-bonding; this manifests itself in a change of the vibrational characteristics, especially the ones documented by the 1st-order spectrum. Thus, in coordinated Raman/SIMS analyses of presolar grains, the Raman analysis of sp^2-bonded carbonaceous samples has to be done before the samples are studied in the ion probe.

2.3. NanoSIMS measurements

The isotopic ratios of $^{12}C/^{13}C$, $^{14}N/^{15}N$, $^{16}O/^{18}O$, and $^{29,30}Si/^{28}Si$ were obtained on all 103 grains with the NanoSIMS. These ratios were determined from measurements of negative secondary ions produced with a Cs^+ primary ion beam. Nitrogen isotopic ratios were obtained from analysis of $^{12}C^{14}N^-$ and $^{12}C^{15}N^-$. In addition, measurements of Mg and Al isotopes as positive secondary ions were performed on the KFA1 and KFB1 grains of this study; Al–Mg measurement of KFC1 grains as well as K, Ca, and Ti isotopic measurements of grains from all density fractions are planned for the future. Preliminary isotopic results were reported by Xu et al. (2012).

In the present Raman paper, however, we only include the C, N, and O isotopic ratios of the grains (Table 1). Unfortunately, the Si isotopic data suffered from instrumental problems and are therefore not reported. Raman analysis with visible excitation can give information only about the surfaces of the grains. Therefore, we do not expect any future measurements/results of Ti, K Ca isotopes (occurring mostly in interior subgrains) to be relevant for this coordinated NanoSIMS/Raman study, and we consider the isotopic ratios of C, N and O the most relevant SIMS results in the context of the present study.

2.4. Laser Raman microprobe measurements

2.4.1. Instrument

Raman spectra were obtained from 100 to 4000 Δcm^{-1} on optically pre-selected, photo-documented μm-sized areas of round grains. The instrument used is a fiber-optically coupled confocal Raman microprobe (HoloLab Series 5000 Raman Microscope from Kaiser Optical Systems, Inc.), which incorporates a research-grade Leica DML microscope with transmitted and reflected light. The light from a frequency-doubled Nd-YAG laser is delivered via a 8 μm single-mode optical fiber and provides excitation at 532 nm (18,976 cm^{-1}). An 80x objective with a numerical aperture of 0.75 and a working distance of 8 mm was used for focusing the light onto the sample, which resulted in a laser spot size (and thus a spatial resolution) of ~1 μm. The laser power at the surface was less than 0.2 mW. The backscattered light (including the Raman scattered light) is collected through the same 80x objective used for delivering the exciting laser beam and is focused onto the core of a 100 μm multimode optical collection fiber; it is guided into the spectrometer configured with a Holoplex transmission grating (HPG-532), which splits the collected signal into two beams that are imaged onto a thermoelectrically-cooled 2048 channel CCD array detector. The spectrometer geometry is such that the 100–2500 Δcm^{-1} region is imaged onto the upper part of the detector, and the 2500–4400 Δcm^{-1} region is imaged onto the lower part. This optical design permits the whole Raman spectral region (i.e., 100–4000 Δcm^{-1}) to be detected simultaneously with a spectral resolution of ~2.5 cm^{-1}. Absolute wavenumber calibration is performed with the lines of Ne and Ar emission lamps. Relative wavenumber calibration is obtained with cyclohexane and monitored twice a day by analyzing a (100) Si

Table 1
Murchison sp^2-bonded carbon grains from three different density fractions studied with MicroRaman and NanoSIMS.

Grain#	Size (μm)	Morphology	Raman type	D/G ratio	$^{12}C/^{13}C$	$^{12}C^{14}N/^{12}C^{15}N$	$^{16}O/^{18}O$
KFA1 Grains (low density)							
[0,4]	3.3	cauliflower	glassy	1.14	91.4 ± 0.5	268.8 ± 2.2	516.9 ± 9.5
[1,2]a	**5.1**	**cauliflower**	**disord. graph**	**0.70**	**91.3 ± 0.5**	**257.3 ± 4.9**	**494.2 ± 11.3**
[1,2]b-2	3.4	cauliflower	disord. graph	0.85	35.3 ± 0.2	262.3 ± 2.3	264.0 ± 3.9
[2,1]	**4.3**	**cauliflower**	**disord. graph**	**0.96**	**91.3 ± 0.5**	**101.6 ± 0.9**	**81.5 ± 1.0**
[3,00]a	13.0	onion	graph	0.20	7.5 ± 0.1	271.4 ± 3.7	500.3 ± 10.9
[3,00]b	3.3	onion	graph	0.21	1773.9 ± 13.3	227.3 ± 2.6	489.1 ± 9.2
[3,2]	**2.9**	**cauliflower–onion**	**glassy**	**1.43**	**101.7 ± 0.6**	**203.7 ± 6.2**	**412.0 ± 14.8**
[3,3]	3.1	onion	disord. graph	0.50	n.d.	n.d.	n.d.
[5,0]a	**3.1**	**onion**	**disord. graph**	**1.09**	**44.2 ± 0.2**	**303.7 ± 6.6**	**228.3 ± 3.8**
[5,0]b	**2.9**	**cauliflower**	**disord. graph**	**1.03**	**93.4 ± 0.6**	**255.4 ± 4.7**	**498.9 ± 8.6**
[5,3]a	**6.0**	**cauliflower**	**disord. graph**	**1.02**	**92.1 ± 0.5**	**256.6 ± 4.4**	**503.1 ± 7.6**
[5,6]	**2.9**	**cauliflower**	**disord. graph**	**1.02**	**80.8 ± 0.5**	**236.6 ± 2.8**	**493.0 ± 6.0**
[6,00]	**6.9**	**cauliflower**	**disord. graph**	**1.06**	**37.5 ± 0.2**	**179.9 ± 3.5**	**359.5 ± 6.7**
[6,1]	4.5	cauliflower–onion	disord. graph	1.02	341.2 ± 2.0	128.6 ± 1.3	410.8 ± 6.8
[6,2]	**3.6**	**cauliflower–onion**	**glassy**	**1.28**	**25.3 ± 0.2**	**118.4 ± 1.6**	**486.0 ± 6.2**
[6,3]	**3.7**	**cauliflower**	**disord. graph**	**0.54**	**91.0 ± 0.5**	**185.4 ± 2.6**	**507.7 ± 8.2**
[6,4]	**4.9**	**onion**	**disord. graph**	**0.92**	**928.8 ± 6.2**	**253.1 ± 2.8**	**234.1 ± 3.4**
[6,6]	n.d.	n.d.	disord. graph	0.81	21.0 ± 0.1	245.9 ± 4.0	490.7 ± 9.9
[7,4]a	3.6	cauliflower	disord. graph	0.90	75.1 ± 2.9	194.1 ± 5.1	477.8 ± 5.6
[7,4]b	3.0	cauliflower–onion	disord. graph	0.81	347.3 ± 2.1	301.7 ± 10.0	449.1 ± 10.7
[7,6]	**3.8**	**cauliflower**	**disord. graph**	**0.76**	**91.1 ± 0.5**	**245.7 ± 5.2**	**495.0 ± 10.4**
$n = 21$ KFA1 grains are graphitic and/or glassy				**$x = 0.87 \pm 0.31$**	terr = 89	air = 272	terr = 499
[4,6]	3.4	cauliflower–onion	kerogen	n.d.	479.3 ± 1.4	280.6 ± 9.4	491.6 ± 22.6
[6,5]		n.d.	kerogen	n.d.	8.7 ± 0.0	159.5 ± 2.3	516.4 ± 10.5
[7,5]	3.5	cauliflower	kerogen	n.d.	108.4 ± 5.1	220.8 ± 5.5	457.0 ± 5.5
KFB1 Grains (medium density)							
[0,2]a	**4.7**	**cauliflower–onion**	**graph**	**0.30**	**592.1 ± 1.2**	**277.9 ± 2.8**	**499.2 ± 10.1**
[0,2]b	3.8	cauliflower	disord. graph	0.77	80.4 ± 0.4	272.5 ± 2.8	498.2 ± 10.6
[0,5]a	3.8	cauliflower	graph	0.44	149.0 ± 0.2	267.6 ± 2.2	504.8 ± 10.3
[0,5]b	3.8	cauliflower	glassy	1.26	49.9 ± 0.2	275.7 ± 2.4	501.7 ± 8.6
[0,6]a	7.5	cauliflower–onion	graph	0.17	2285.1 ± 10.4	269.3 ± 4.2	518.9 ± 11.5
[0,6]b	4.9	cauliflower–onion	graph	0.24	216.6 ± 0.9	270.1 ± 2.7	490.5 ± 9.2
[1,2]a2	3.8	cauliflower–onion	graph	0.16	883.2 ± 2.3	277.4 ± 4.8	522.7 ± 14.2
[1,2]b1	3.4	cauliflower	disord. graph	0.80	1867.8 ± 11.5	273.4 ± 3.3	495.0 ± 10.5
[1,2]b2	3.1	cauliflower	graph	0.41	383.5 ± 0.7	273.8 ± 2.9	505.4 ± 10.8
[1,3]	8.9	cauliflower–onion	graph	0.36	297.1 ± 1.7	274.7 ± 2.5	514.3 ± 10.1
[2,1]b	6.2	onion	disord. graph	0.64	12.1 ± 0.1	272.6 ± 2.5	504.9 ± 10.0
[2,1]d1	4.6	cauliflower–onion	graph	0.38	333.8 ± 0.6	266.3 ± 4.1	516.4 ± 16.5
[2,7]	4.8	cauliflower	graph	0.31	670.6 ± 3.2	272.3 ± 2.4	526.3 ± 10.6
[3,7]a	**5.9**	**cauliflower**	**disord. graph**	**0.86**	**136.1 ± 0.6**	**274.4 ± 2.6**	**533.9 ± 9.9**
[3,7]b	3.8	onion	graph	0.21	532.5 ± 2.5	273.5 ± 2.6	512.6 ± 10.0
[3,7]c	4.0	cauliflower	disord. graph	0.51	91.2 ± 0.4	270.6 ± 2.8	498.2 ± 10.5
[4,1]a	**3.8**	**cauliflower**	**disord. graph**	**0.50**	**627.9 ± 2.9**	**272.1 ± 3.9**	**492.0 ± 10.0**
[4,1]b	**3.0**	**onion**	**graph**	**0.33**	**286.1 ± 1.2**	**268.7 ± 3.2**	**493.9 ± 11.1**
[4,3]	4.1	onion	graph	0.20	565.3 ± 2.7	265.8 ± 2.2	499.4 ± 9.8
[4,7]a	3.5	cauliflower–onion	disord. graph	0.79	676.6 ± 3.2	273.0 ± 2.9	493.3 ± 10.8
[4,7]c	**4.2**	**cauliflower–onion**	**graph**	**0.24**	**66.6 ± 0.3**	**266.3 ± 3.8**	**499.1 ± 10.8**
[4,7]e	6.2	cauliflower	disord. graph	0.53	948.8 ± 5.3	266.0 ± 5.0	494.3 ± 15.2
[4,7]i	4.5	onion	graph	0.20	795.8 ± 4.0	267.5 ± 3.3	490.3 ± 11.3
[4,7]j	5.4	onion	graph	0.22	164.9 ± 0.7	272.5 ± 2.7	488.0 ± 10.2
[5,0]	**5.0**	**cauliflower–onion**	**graph**	**0.27**	**257.3 ± 1.1**	**268.7 ± 3.2**	**515.7 ± 11.5**
[5,2]a	**4.0**	**onion**	**graph**	**0.18**	**873.3 ± 4.4**	**263.9 ± 2.7**	**510.9 ± 11.2**
[5,2]c	3.4	cauliflower–onion	graph	0.48	90.1 ± 0.4	263.2 ± 3.7	491.4 ± 11.6
[5,6]a	3.3	onion	disord. graph	0.86	486.8 ± 2.2	271.3 ± 2.7	505.8 ± 10.9
[5,6]e	5.5	onion	graph	0.31	207.6 ± 0.9	272.1 ± 2.7	494.6 ± 10.8
[6,2]a1	**4.6**	**onion**	**graph**	**0.38**	**986.6 ± 4.7**	**267.3 ± 3.5**	**490.5 ± 12.0**
[6,2]b	**3.0**	**cauliflower**	**disord. graph**	**0.60**	**90.7 ± 0.4**	**270.4 ± 4.0**	**493.1 ± 10.6**
[6,2]c	**4.0**	**cauliflower**	**disord. graph**	**0.64**	**90.0 ± 0.4**	**267.4 ± 3.5**	**500.0 ± 12.3**

(*continued on next page*)

Table 1 (*continued*)

Grain#	Size (μm)	Morphology	Raman type	D/G ratio	$^{12}C/^{13}C$	$^{12}C^{14}N/^{12}C^{15}N$	$^{16}O/^{18}O$
[6,3]	**3.2**	**onion**	**graph**	**0.16**	**90.2 ± 0.4**	**265.7 ± 2.6**	**482.5 ± 10.1**
[6,4]	3.4	cauliflower–onion	graph	0.25	214.6 ± 0.9	268.2 ± 2.2	507.7 ± 9.9
[7,1]o	4.9	onion	graph	0.28	623.9 ± 3.1	271.4 ± 2.6	507.5 ± 8.1
[7,3]a	**3.8**	**cauliflower**	**disord. graph**	**0.78**	**90.2 ± 0.4**	**270.4 ± 3.3**	**503.2 ± 9.1**
[7,3]b	3.0	onion	graph	0.32	1102.8 ± 6.0	273.0 ± 2.7	501.5 ± 8.1
[7,6]o	4.0	onion	graph	0.24	106.3 ± 0.4	266.1 ± 2.6	486.1 ± 7.6
$n = 38$ KFB1 grains are graphitic and/or glassy				**$x = 0.44 \pm 0.26$**	terr = 89	air = 272	terr = 499
[6,5]	3.4	cauliflower–onion	kerogen	n.d.	9.0 ± 0.1	269.3 ± 2.5	490.0 ± 10.1
[6,7]	3.7	cauliflower–onion	kerogen	n.d.	498.8 ± 2.3	270.4 ± 4.2	485.3 ± 11.2
[7,5]	3.2	cauliflower–onion	kerogen	n.d.	993.5 ± 5.1	264.3 ± 2.6	503.0 ± 10.9
KFC1 Grains (high density)							
[0,1]	2.9	cauliflower	disord. graph & fluor	0.74	90.9 ± 0.3	263.7 ± 2.3	503.5 ± 9.1
[0,2]a	**3.7**	**onion**	**graph & fluor**	**0.15**	**705.0 ± 3.2**	**256.0 ± 2.3**	**487.3 ± 8.5**
[0,3]a	3.9	onion	graph & fluor	0.33	17.9 ± 0.2	305.6 ± 2.8	472.7 ± 7.4
[0,3]b	3.9	cauliflower–onion	graph	0.23	1222.9 ± 9.3	255.4 ± 3.5	501.9 ± 9.8
[0,3]c	3.3	onion	graph	0.43	16.0 ± 0.2	241.4 ± 4.0	488.9 ± 7.0
[0,6]a	**4.1**	**onion**	**graph & fluor**	**0.23**	**493.9 ± 1.8**	**262.7 ± 3.3**	**499.3 ± 9.1**
[0,6]b	3.1	cauliflower	graph	0.15	520.8 ± 2.5	269.6 ± 6.9	508.7 ± 11.0
[1,0]	3.2	onion	disord. graph	0.54	3132.2 ± 47.8	250.8 ± 4.4	493.4 ± 10.3
[1,4]	2.9	onion	graph	0.15	726.1 ± 3.1	268.2 ± 2.4	486.2 ± 8.0
[1,7]a	**4.4**	**cauliflower–onion**	**graph**	**0.21**	**2025.3 ± 16.0**	**268.2 ± 3.7**	**480.1 ± 8.0**
[2,0]	5.1	onion	graph	0.23	74.9 ± 0.3	252.9 ± 2.7	485.5 ± 15.5
[2,5]	2.6	unknown	unusual	1.23	254.7 ± 0.8	257.4 ± 4.7	511.1 ± 12.8
[3,5]a	3.3	cauliflower–onion	graph & fluor	0.26	102.5 ± 0.3	267.0 ± 2.1	454.8 ± 6.6
[3,5]b	**5.3**	**cauliflower–onion**	**graph & fluor**	**0.16**	**239.7 ± 0.8**	**265.4 ± 2.6**	**496.6 ± 10.3**
[3,6]	**3.8**	**onion**	**graph**	**0.12**	1759.5 ± 12.7	275.4 ± 3.8	494.6 ± 10.2
[3,7]o	3.6	onion	graph	0.30	237.6 ± 0.8	269.5 ± 2.9	490.5 ± 8.6
[4,7]	3.4	onion	graph	0.28	421.7 ± 2.0	268.0 ± 5.6	491.6 ± 12.5
[5,00]b	3.7	cauliflower–onion	disord. graph	0.87	6.5 ± 0.1	210.3 ± 3.7	468.4 ± 10.0
[5,0]a	3.5	cauliflower–onion	graph & fluor	0.25	473.7 ± 2.0	269.4 ± 2.0	494.9 ± 7.7
[5,0]b	**3.4**	**onion**	**unusual**	**1.08**	**550.9 ± 2.2**	**234.4 ± 2.8**	**484.8 ± 8.6**
[5,2]a	**5.2**	**cauliflower–onion**	**graph & fluor**	**0.19**	**689.7 ± 3.3**	**271.9 ± 2.2**	**493.0 ± 8.8**
[5,2]b	**5.9**	**onion**	**graph & fluor**	**0.31**	**761.2 ± 3.8**	**269.8 ± 2.2**	**490.8 ± 8.3**
[5,2]c	**4.3**	**cauliflower**	**graph**	**0.20**	**869.6 ± 4.0**	**273.6 ± 3.7**	**494.2 ± 8.6**
[5,3]a	**3.4**	**onion**	**graph & fluor**	**0.35**	**181.6 ± 0.6**	**260.1 ± 2.4**	**482.7 ± 7.5**
[5,6]	3.4	onion	graph	0.18	426.9 ± 1.7	260.3 ± 3.9	498.8 ± 9.6
[6,1]a	2.9	onion	graph	0.13	268.2 ± 0.9	262.3 ± 4.2	488.7 ± 10.0
[6,1]b	3.1	cauliflower–onion	graph	0.36	9.4 ± 0.1	258.4 ± 7.4	505.3 ± 16.0
[6,2]a	2.9	cauliflower–onion	graph & fluor	0.26	174.2 ± 0.5	267.3 ± 2.1	492.4 ± 8.2
[6,2]b	3.8	cauliflower–onion	graph	0.20	209.7 ± 1.0	269.4 ± 4.4	487.5 ± 8.0
[6,2]c	4.3	onion	graph	0.12	877.4 ± 4.5	267.3 ± 2.9	503.1 ± 9.1
[6,7]a	3.3	onion	disord. graph & fluor	0.51	15.2 ± 0.2	268.8 ± 5.9	476.5 ± 12.7
[6,7]b	3.3	cauliflower–onion	unusual & fluor	0.67	430.5 ± 1.8	263.6 ± 2.9	496.1 ± 9.9
[7,1]	**4.8**	**onion**	**graph**	**0.24**	**61.7 ± 0.2**	**266.6 ± 3.1**	**496.9 ± 9.1**
[7,2]a	2.7	onion	unusual	0.33	395.3 ± 1.3	263.1 ± 3.9	506.5 ± 10.6
[7,4]a	**3.5**	**onion**	**graph**	**0.25**	**431.1 ± 1.7**	**265.4 ± 2.4**	**498.0 ± 8.5**
[7,4]b	4.3	onion	graph	0.25	690.9 ± 3.1	271.3 ± 2.7	500.6 ± 9.3
$n = 36$ KFC1 grains are graphitic and/or glassy				**$x = 0.35 \pm 0.26$**	terr = 89	air = 272	terr = 499
[1,7]b	4.4	cauliflower–onion	kerogen	n.d.	n.d.	n.d	n.d.
[5,00]a	4.2	onion	kerogen	n.d.	9.5 ± 0.1	103.8	486.0

n.d ….not determined; grains whose spectra are shown in Fig. 7 are printed in bold; errors are 1σ.
Raman types: Int_D / $Int_G < 0.5$ = "**graphite**"; $0.51 < Int_D/Int_G < 1.1$ = "**disord**ered **grap**hite"; $Int_D/Int_G > 1.1$ = "**glassy** carbon".
"fluor"…. Raman bands are superimposed on broad laser-induced fluorescence background.
"unusual"…... second-order Raman peaks are unusually intense relative to first-order bands.

wafer whose recorded peak position is $520.6 \pm 0.1\ \Delta cm^{-1}$. Further instrumental details can be found in Wopenka (2012).

For the analysis of presolar grains of the present study, the spectral acquisition time of each micrometer-sized spot was ~ 4 min (256 s, to be exact) per spectrum. Each grain was analyzed at least 3 times in a micrometer-sized spot onto which the exciting laser beam was individually focused. An attempt was made to analyze different μm-sized areas of a given grain, but for the smaller grains there

probably was some overlap in the excitation volume of individual Raman measurements. But in any case, all the spectra obtained on a given grain were characteristic for that grain; in order to increase the signal-to-noise ratio, the spectra shown in the figures are typically the sums of 2–5 individually acquired spectra for a given grain. The state of the samples seemed to be unchanged by the Raman analysis. At least no damage could be visually recognized via optical microscopy. All spectra shown are plotted as raw spectra, i.e., no baseline-correction was applied. Raw spectra are preferred, because they do not only give information about the Raman bands, but also about the laser-induced fluorescence of the sample. The latter is manifested in high background count rates that typically increase with increasing relative wavenumber. In the present study of individual Murchison presolar grains, laser-induced fluorescence was not a big problem: it either did not exist (for KFA1, KFB1, and for most of the KFC1 grains), or it was not very strong (for 1/3 of the KFC1 grains; Table 1).

The excitation depth and excitation volume in a Raman microprobe analysis depend not only on the objective used, but also on the optical properties of the sample. Carbonaceous materials with sp^2-bonds are highly absorbing at visible wavelengths, and this means that for the excitation wavelength used (532 nm) the laser light is totally absorbed in the top ~100 nm surface layer of the sample. Therefore, the Raman spectrum of an individually mounted presolar graphite grain can only give information about its surface. The only way to obtain information about the chemistry and/or structure of the interior of the grains via Raman spectroscopy is to ultra-microtome individual grains (similar to what is required for TEM studies), place them on a Cu, Ni or Au grid or silicon wafer, and analyze several 50–90 nm thick slices of each grain (Groopman et al., 2012a). However, such complicated sample preparations were not done for the grains of the present study.

2.4.2. Crystallinity, disorder, and nomenclature of sp^2-bonded materials

The structural terms "disorder" and "degree of crystallinity" of carbonaceous materials as used by different authors are often not well defined, and can have different meanings when they are used in the context of different analytical techniques. This can lead to misunderstandings, such as the use of the term "graphite" for materials that are not confirmed to have a well-defined crystallographic order, or even the use of contradictory terms such as "amorphous graphite" (Schopf et al., 2002). It also is not always clear what is being called "graphite" in TEM studies; for instance in the study of Bernatowicz et al. (1991), presolar carbon grains with short, curved and discontinuous layers of graphene sheets that lack long-range continuity are called "scaly cauliflower graphite". Such nanocrystalline materials are probably the same kind of materials as the ones that are called "glassy carbon" (and considered amorphous) in the Raman spectroscopic literature (e.g., Nakamizo et al., 1974; McCulloch and Prawer, 1995; Escribano et al., 2001; Tao et al., 2011), as well as in studies performed by neutron diffraction (Mildner and Carpenter, 1982) and X-ray photoemission (McFeely et al., 1974). Because of this confusing situation of differing nomenclatures and the fact that different techniques are sensitive to different aspects of the crystallographic lattice and its ordering, the following is a brief summary of the crystallographic aspects of sp^2-bonded carbon.

In a well-crystalline graphite crystal (1) the condensed benzene rings (6-fold rings of carbon atoms, whose electrons are arranged in-plane via 2s, $2p_x$ and $2p_y$ (sp^2) orbitals), extend at least tens to hundreds of nanometers within the basal plane; the measured parameter along the *a*-axis is the crystal size L_a; the shortest interatomic covalent bond distance in the plane is 0.142 nm; and (2) the basal planes are spaced equidistantly (with an interplanar spacing $d_{(002)}$ of exactly 0.335 nm) in stacks that also extend at least tens to hundreds of nanometers; the measured parameter along the *c*-axis is the crystal size L_c. The size of the ordered graphite domains (i.e., L_a and L_c) is referred to as the crystallite size or "basic structural units". Solid carbon phases that have crystalline order, but with $d_{(002)} > 0.335$ nm and/or crystallite sizes L_a and L_c that are smaller than several hundreds of nanometers are often referred to as "disordered graphites". The covalent bond distance of 0.142 nm is always preserved, even in "disordered graphites". The information that can be obtained from the 1st-order Raman spectrum is related to the in-plane crystallite size L_a, and graphite is called "disordered" when L_a is smaller than ~400 nm (Tuinstra and Koenig, 1970). The weak interlayer bonding between different basal sp^2-bonded planes (i.e., "graphene sheets") allows for variations in interplanar spacings ($0.31\ \text{nm} < d_{(002)} < 0.39\ \text{nm}$), which is one of the structural parameter that indicates "order and disorder" in TEM analyses. It frequently seems to be the case that if the crystallite size is small (both in terms of L_a and/or L_c), then the interplanar spacings are rather wide. When the interplanar spacing becomes >0.335 nm, then a loss of three-dimensional crystallinity is observed. When the layers of graphene stay perfectly parallel, but their mutual orientation in the direction of the planes is random, the material is called "turbostratic graphite" in TEM-related research. Such turbostratic graphite is described as consisting of discrete fragments of curved stacked carbon sheets lacking long-range continuity (Croat et al., 2008), and this seems to be the same type of material that is referred to as "glassy carbon" in the Raman literature. Synthetically produced glassy carbons are known to be non-graphitizing and chemically very resistant, and it was suggested that they have fullerene-related microstructures, i.e., that they contain pentagons and heptagons as well as hexagons within their sp^2-bonded sheets of carbon (Harris, 2004).

It was already realized by Tuinstra and Koenig (1970) that the frequency of the Raman-active E_{2g} mode (i.e., the so-called G peak) does not depend on the mutual arrangement of the graphite planes (despite the fact that those authors had the actual frequency wrong; they reported 1575 Δcm^{-1} instead of 1582 Δcm^{-1}), and that this peak appears at the same position in any form of sp^2-bonded carbon. They also had realized that a second strong peak (the so-called D peak around 1350 Δcm^{-1}) appears for samples with a small crystallite size (<several hundreds of nm), and that the D/G peak intensity ratio is inversely correlated with the lateral dimension L_a of the crystallites.

Empirically, it is recognized that the D peak becomes not only Raman active for small crystallite sizes, but also in the presence of anything else that breaks the translational symmetry of the crystal, i.e., structural defects and impurities. It is also recognized that there is another defect-induced peak (D′ at ~1620 Δcm^{-1}), a strong second-order (two-phonon peak; 2D peak) at ~2720 Δcm^{-1}, and several less intense second-order peaks (D + D′ at ~2445 Δcm^{-1} and 2D′ at ~3248 Δcm^{-1}) that occur in most sp^2-bonded carbon materials (e.g., Tan et al., 2004; Beyssac and Lazzeri, 2012). Peculiar aspects of those defect-induced peaks are that the frequency of the first-order D peak depends on the excitation wavelength, and that the various second-order peaks are also present in well crystalline graphite, which does not have any defect-induced first-order D peak (Fig. 2a). It is also recognized that the width/shape of the 2D peak at ~2720 Δcm^{-1} is related to the three-dimensional ordering of the carbonaceous material; in turbostratic graphite, the second-order 2D peak is very similar to the 2D peak for two-dimensional graphene, i.e., narrow and very symmetric with a Lorentzian shape (Ferrari et al., 2006). In contrast, the 2D peak for three-dimensional crystalline graphite is asymmetric, much wider and can be resolved into at least two components (Lespade et al., 1984). Thus, the shape and/or symmetry of the 2D peak ~2720 Δcm^{-1} is recognized to provide some information on the stacking order of the sp^2-bonded carbonaceous material; the observed spectral differences are caused by differences in the electronic band structures between graphene/turbostratic graphite and crystalline graphite, respectively. Amazingly, however, even though the defect-induced peaks have been observed in the Raman spectra for decades, their origins and behaviors still cannot (yet) fully be explained theoretically. After Tunistra and Koenig's landmark paper from more than 40 years ago, the sp^2-hybridized carbon–carbon bond remains the bond most studied in the Raman literature. As pointed out by Dresselhaus et al. (2010), "carbon has been investigated for more than half a century without exhausting its wonders and challenges". Many excellent discussions about the current theoretical understanding of this bond are available (e.g., Dresselhaus et al., 1999; Ferrari and Robertson, 2000; Reich and Thomsen, 2004; Ferrari, 2007). The now most commonly accepted theory for the origin, assignment, position and dispersive behavior of the various disorder-induced peaks seems to be based on the double-resonance theory (Thomsen and Reich, 2000), which is explained very well (to the non-theoretical physicist) in the recent review by Beyssac and Lazzeri (2012). The present paper, however, is only concerned with empirical aspects of the observed Raman spectra of presolar carbon grains.

2.4.3. Types of Raman spectra of sp^2-bonded carbonaceous materials

Raman spectroscopy can easily distinguish between sp^3- and sp^2-bonded carbon. Well-crystalline sp^3-bonded carbon (i.e., diamond) has one extremely strong 1st-order peak at 1332 Δcm^{-1} and no 2nd-order peaks, whereas well-crystalline sp^2-bonded carbon (i.e., graphite) has a 1st-order peak at 1582 Δcm^{-1}, (traditionally called the G peak for "graphite") and several 2nd-order peaks (Fig 2a). But in addition, Raman spectroscopy is also sensitive to subtle differences in the sp^2 carbon–carbon bonds. Fig. 2b shows Raman spectra for three different terrestrial sp^2-bonded

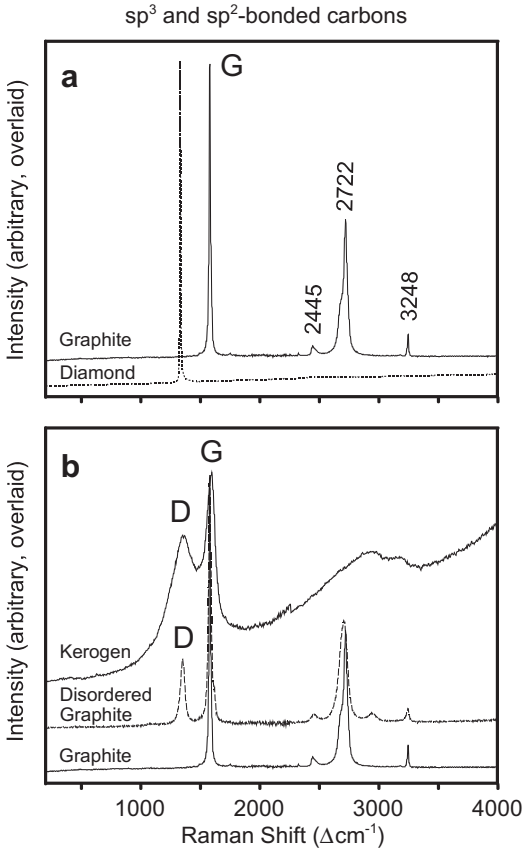

Fig. 2. Raman spectra for different carbon–carbon-bonded materials. All spectra are shown as raw spectra (i.e., without any baseline-corrections), stacked along the *y*-axis for better display, and with arbitrary intensities plotted on the *y*-axes (i.e., absolute differences in peak intensities cannot be seen). They were obtained from terrestrial samples: a diamond wedding ring, Ceylon graphite, graphite in a metamorphic rock, and a Precambrian kerogen sample. (a) Differences between sp^2-bonded carbon and sp^3-bonded carbon. Well crystalline sp^3-bonded diamond has one single extremely strong peak at 1331 Δcm^{-1}, whereas well-crystalline sp^2-bonded graphite has a strong 1st-order peak (G peak for "graphite") at 1582 Δcm^{-1}, and 2nd-order peaks at 2445, 2722 and 3248 Δcm^{-1}. (b) Differences between different sp^2-bonded carbons: a perfectly well-crystalline graphite (mm-sized single crystal of Ceylon graphite), a slightly disordered graphite (sample 71–6 from Grew (1974) isolated from a phyllite with chlorite/biotite grade; estimated L_a ~9 nm (Wopenka and Pasteris, 1993), and an amorphous sp^2-bonded organic carbon (kerogen 114-1-RK in shale sample from Wedeking and Hayes, 1983). Crystalline graphites with disorder (i.e., with in-plane crystallite sizes of <~400 nm, according to the Tuinstra and Koenig (1970) calibration), have, in addition to the G peak, a second narrow peak in the 1st-order spectrum (called D peak for "disorder") at ~1350 Δcm^{-1}, strong 2nd-order peaks and a flat background. Amorphous sp^2-bonded carbonaceous materials, on the other hand, have extremely wide 1st-order peaks, no (or very subdued) 2nd-order peaks, and often strong laser-induced fluorescence.

carbonaceous materials: Well-crystallized Ceylon graphite, not so well crystallized (or "disordered") metamorphic graphite, and amorphous (i.e., not at all crystallized) "macromolecular carbon" or "organic carbon". In imperfectly crystallized sp^2-bonded carbon there appears a second narrow 1st-order peak, the D (for "disorder") peak at $\sim$1350 Δcm^{-1} (exact position depends on the wavelength of excitation laser). The spectrum of amorphous carbon (referred to as "kerogen-type spectrum") has very wide 1st-order peaks, and has no (or very weak) 2nd-order peaks (Fig. 2b); it is typical of terrestrial kerogens and coals (Wopenka and Pasteris, 1993; Quirico et al., 2005a), but it also is typical of vapor-deposited sputtered carbon, soot, activated charcoal, and large polycyclic aromatic hydrocarbons (PAHs). "Kerogen-type" or "PAH-type" Raman spectra are also typical of the matrix and the insoluble organic matter of many meteorites (Bonal et al., 2006, 2007; Busemann et al., 2007; Dobrica et al., 2011; Piani et al., 2012), as well as of interplanetary dust particles (Allamandola et al., 1987; Wopenka, 1988; Quirico et al., 2005b) and returned samples from the Stardust Mission (Rotundi et al., 2008; Wopenka, 2012). Such materials with kerogen-type spectra can be either chemically pure carbon (such as vapor-deposited sputtered carbon), or they can contain various elements such as N, O, H, S (called "heteroatoms") in addition to sp^2-bonded carbon, and thus have C–H, C=O, C–N bonds etc. in addition to sp^2-hybridized C–C bonds. However, due to the unusually strong Raman scattering efficiency of the sp^2-bonded C–C, the Raman bands due to the sp^2 carbon bond will always dominate the spectrum; other bonds (e.g., C–H, C=O, C–N) have much lower Raman scattering efficiencies and their Raman peaks are often below detection limits in the presence of sp^2-bonded carbon. Therefore, the absolute (i.e., peak heights) or integrated (i.e., peak areas) intensities of the sp^2-bonded C–C peaks do not give any information about the absolute or relative abundance of this bond in the analyzed volume of the sample.

Tuinstra and Koenig (1970) were first in realizing that the ratio of the intensities of the two peaks in the 1st-order Raman spectrum of crystalline sp^2-bonded carbon (i.e., the so-called D- and G-peaks, see Fig. 2b) is correlated with the in-plane crystallite size L_a. Their empirical correlation, based on Raman D/G peak height ratios and L_a dimensions indirectly derived from X-ray diffraction (XRD) measurements, and the terms "disordered graphite" or "disordered carbonaceous material" were originally established and used only for graphitic carbon, i.e., for materials that are sp^2-bonded carbon phases of essentially condensed benzene rings, but that also have a 3-dimensional crystalline structure. The Raman spectra of such disordered graphites have narrow 1st-order peaks and strong narrow 2nd-order peaks (Fig. 3a). Their D/G peak intensity ratios can vary, and this ratio is a function of the in-plane crystallite size L_a of the graphitic material. The materials whose spectra are shown in Fig. 3a have various degrees of structural disorder, i.e., different dimensions of in-plane crystallite sizes. However, it has to be kept in mind that the L_a dimensions that are expressed by varying D/G ratios are all fairly small (for instance, they range from 3 to 13 nm for the spectra shown in Fig. 3a; data from Wopenka and Pasteris, 1993).

There exist different methods to determine the peak intensity (integrated or not). Peak area determination via deconvolution routines can suffer from large errors, especially when the peaks are very wide and/or of different widths such as in amorphous sp^2-bonded materials, which produce "kerogen-type spectra". In addition, for most disordered graphites it is necessary to consider the areas of two small peaks in addition to the ones of the D and G peaks in order to reproduce the spectral envelope (as discussed in detail by e.g., Beyssac et al., 2002). Therefore, the most straightforward method to determine D/G peak intensity ratios for graphitic sp^2-bonded carbons is to use maximum peak intensities (i.e., peak heights; Fig. 3b), rather than to deconvolve peaks and determine integrated intensities (i.e., peak areas). The historic Tuinstra and Koenig calibration is based on peak heights, a decision that most likely was triggered by the fact that the software for peak deconvolutions and peak area calculations was not yet available in the 1960s/70s. According to the original Tuinstra and Koenig (1970) calibration (which was later confirmed with direct L_a measurements via TEM studies by Beny-Bassez and Rouzaud, 1985), the ratio $Int_D/Int_G = 0$ when L_a is at least $\sim$ 400 nm, Int_D/Int_G $\sim$0.2 when L_a $\sim$20 nm, and Int_D/Int_G $\sim$1 when L_a $\sim$3 nm; their calibration curve has a very steep slope (i.e., is very sensitive) for L_a dimensions between $\sim$4 and 20 nm (as seen in the spectra shown in Fig. 3a, which cover a large range of D/G ratios, yet a small range in crystallite sizes), and is very flat (i.e., very insensitive) for L_a values $>$ 100 nm. Of note is that Tuinstra and Koenig (1970) originally referred to any kind of carbon material that showed a D peak in its Raman spectrum as "disordered graphite", even if the Int_D/Int_G ratio was extremely small; this original nomenclature was also used in the 1993 paper by Wopenka and Pasteris (spectra shown in Fig. 3a). It is nowadays well recognized, however, that almost any kind of natural graphitic material will have a small D peak. Therefore, in the present work, samples with $Int_D/Int_G < 0.5$ are not yet referred to as "disordered", but rather are considered still "fairly well ordered graphite" (see discussion below).

As mentioned above, the material that is referred to as "disordered graphite" (Fig. 3a) has spectra with narrow 1st- and 2nd-order peaks in which the D peaks are less intense than the G peaks ($Int_D < Int_G$). There is also the possibility that the peaks are narrow (even though not quite as narrow as in disordered graphite) but with $Int_D > Int_G$. This type of spectrum is obtained from a synthetically produced nano-crystalline material called "glassy carbon". An example for the spectrum of naturally occurring "glassy carbon" (IOM of the Allende meteorite) is shown in Fig. 3c; note that the 2nd order peaks of glassy carbon are less intense and different from the ones for disordered graphites (compare Fig. 3a and c).

3. RESULTS AND DISCUSSION

3.1. Surface morphology

Presolar graphite grains have been classified based on their surface morphology as observed in SEM images.

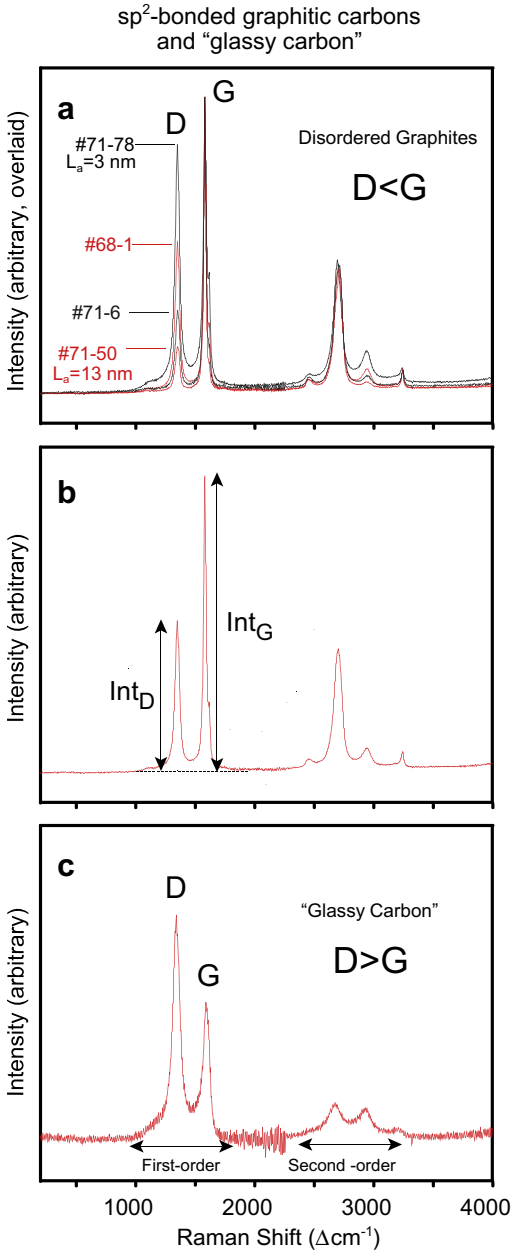

Fig. 3. First and 2nd-order Raman spectra of sp^2-bonded graphitic carbon with different degree of disorder, and of so-called "glassy carbon". (a) Raw spectra obtained from four different disordered graphitic samples (from different metamorphic terrestrial rocks). Different degrees of structural disorder can be seen in the differences of the D/G peak intensity ratios (Int_D/Int_G). Spectra are normalized to the G band. The stronger the D ("disorder) peak at ~1350 Δcm^{-1} relative to the G ("graphite") peak at ~1582 Δcm^{-1}, the smaller is the in-plane crystallite size L_a of graphite. Disordered graphites have 3-dimenional crystalline structure, and thus their Raman spectra have 2nd-order peaks. Raw Raman spectra of the crystalline inorganic sp^2-bonded carbon samples (i.e., graphites) have typically flat backgrounds (i.e., no fluorescence is induced by the laser beam), even if they are disordered. Spectra are shown for a range of in-plane crystallite sizes for the following metamorphic graphitic samples: #71–78 (chlorite grade with $Int_D/Int_G = 0.74$); #68-1 (garnet grade with $Int_D/Int_G = 0.40$); #71-6 (chlorite/biotite grade with $Int_D/Int_G = 0.29$); #71-50 (staurolite grade with $Int_D/Int_G = 0.14$); data from Wopenka and Pasteris (1993), obtained with 514 nm excitation. (b) Measurement of Int_D/Int_G peak intensity of disordered graphites; this is the method of intensity ratio measurement the original Tuinstra and Koenig (1970) calibration was based on (rather than on peak areas). The materials referred to as "disordered graphites" in the Raman spectroscopic literature always have more intense G peaks than D peaks ($Int_D < Int_G$). (c) The spectrum of sp^2-bonded material that is referred to as "glassy carbon" in the Raman spectroscopic literature; Glassy carbon is characterized by very narrow 1st-order peaks, but, in contrast to graphitic carbon, with an unusually intense D peak ($Int_D > Int_G$), and subdued second-order peaks.

Originally, presolar graphite grains were classified as "onions" when they had smooth surfaces, and "cauliflowers" when the looked like miniaturized heads of cauliflower (Amari et al., 1993; Zinner et al., 1995). Hoppe et al. (1995) characterized more than 500 Murchison graphite grains from separates KFA1, KFB1, and KFC1 and distinguished

between cauliflowers with coarse surface texture (CF-c), which in this study we call cauliflowers, and cauliflowers with fine surface texture (CF-f), which we call "cauliflower–onions". In addition, in the Hoppe et al. (1995) study 3% of the grains were classified as "other". Additional insights into the appearances and/or structures of presolar graphite came from TEM investigations of ultramicrotomed grains (Bernatowicz et al., 1991, 1996; Croat et al., 2003). Those TEM studies found a general correlation between surface morphology and internal structure, but added other nomenclature terms to better describe the internal morphology/microstructure/crystallographic structure of presolar grains, such as "onions with and without nanocrystalline cores", "platy turbostratic graphites" (with continuous concentric layering and well-developed (002) lattice fringes), and "scaly cauliflower graphites" (with short, curved and discontinuous layers that lack long-range continuity). The grains in the present study, however, were not (yet) studied by TEM, and thus were only classified based on their surface morphology as observed in SEM images. Therefore, we do not know whether the grains in this study had well-crystalline or nanocrystalline cores and whether they had any refractory sub-grains.

We analyzed 24 grains from the low-density fraction KFA1, 41 grains from the medium-density fraction KFB1, and 38 grains from the high-density fraction KFC1. All 103 grains were spherical or ellipsoidal and ranged from 3 to 13 μm in diameter, but most grains were <4 μm (Table 1). The surface morphology of most grains studied in the present work can be unambiguously described as either "onion" or "cauliflower", i.e., smooth spheres as "onions" (O) and "flowery spheres" as "cauliflowers" (CF; see Table 1). However, in all three density fractions there were also many grains whose morphology did not unambiguously define them as onions or cauliflowers, and their morphology classification was very subjective (i.e., different people could/would classify them differently). Those grains fell in between, and we thus named them "cauliflower–onions" (CFO). Please note that grains of this type with mixed or unclear surface morphology were named "caulionions" in the abstract by Xu et al. (2012). Fig. 4 shows the relative abundances of different graphite morphological types among the grains of the present study. The KFA1 density fraction is dominated by grains with cauliflower morphology (12 of 24 grains), whereas the KFC1 density fraction is dominated by grains with onion morphology (22 of 38 grains). All three different morphology types are evenly represented in the medium density fraction KFB1. These distributions qualitatively agree with those of Xu et al. (2012) and Hoppe et al. (1995) but differ in detail, which only demonstrates that there exist no absolute criteria for assessing the surface morphology of presolar graphite grains. Attribution of morphology is quite obvious for the end-members onions and cauliflowers, but cases lying in between are classified differently by different observers. In spite of these differences, the overall conclusions are consistent among different research groups and/or researchers: onions are most abundant in KFC1 and least abundant in KFA1, whereas cauliflowers are most abundant in KFA1 and least abundant in KFC1.

3.2. Raman spectra

3.2.1. Differences and similarities observed among grains of different density

Different types of Raman spectra (graphite, disordered graphite, kerogen-type) were observed for individual presolar grains in all three density fractions; glassy carbon spectra were observed in the KFA1 and KFB1 density fractions; examples of full spectra (i.e., from 400 to 4000 Δcm^{-1}) obtained on KFA1 grains are shown in Fig. 5. Very few grains in all three density fractions had "kerogen-type" spectra with extremely wide 1st-order and weak 2nd-order peaks

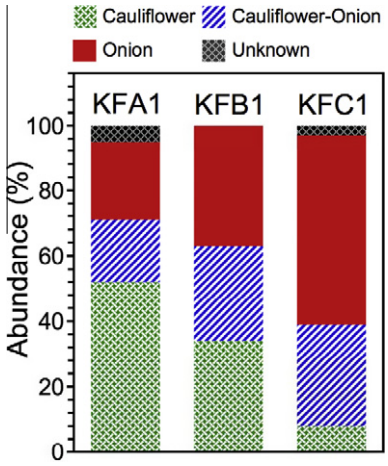

Fig. 4. Relative abundances of different morphological types determined by SEM for 103 presolar graphite grains from different density fractions (KFA1, KFB1, KFC1; Amari et al., 1994) of the Murchison meteorite.

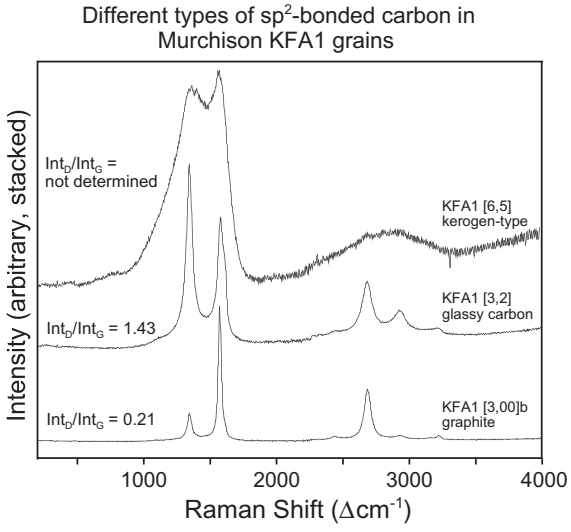

Fig. 5. Three different types of 1st- and 2nd-order Raman spectra (400–4000 Δcm^{-1}) characteristic of sp^2-bonded carbon that are observed from micrometer-sized areas in Murchison presolar grains. Examples are shown for different individual grains from density fraction KFA1, as listed in Table 1.

(see discussion below and Table 1). Kerogen-type spectra were not further interpreted in terms of their D/G intensity ratios. However, the vast majority (95/103) of the grains had spectra with very narrow 1st-order peaks (D and G) and very strong 2nd-order peaks; as explained above, the D/G intensity ratios of those spectra can be used to infer the graphitic in-plane crystallite size, which is one of several parameters indicative of "structural order". Based on their D/G intensity ratios, the grains were grouped into the following Raman types: (fairly well ordered) "graphite" ($Int_D/Int_G < 0.5$), "disordered graphite" ($0.51 < Int_D/Int_G < 1.1$), "glassy carbon" ($Int_D/Int_G > 1.1$), and "unusual sp^2-bonded carbon" (with extremely intense 2nd-order peaks relative to the 1st-order peaks). Please note that this classification is different from the one typically used by Raman spectroscopists, who refer to any material that has a disorder (D) peak (with $Int_D/Int_G < 1$) as "disordered carbonaceous material" or "disordered graphite" (see, e.g., data of terrestrial metamorphic samples shown in Fig. 3). However, based on the fact that almost any kind of natural graphitic material (with the exception of single crystals of natural fluid-deposited graphite) will have a D peak, we find the definition used in the present paper to be more appropriate.

Table 1 gives a summary of the Raman and NanoSIMS results of all three density fractions. Raman spectra characteristic of (fairly well ordered) "graphite" and "disordered graphite" are found for grains of all three density fractions, but in very different abundances (Fig. 6). Whereas most low-density grains (KFA1) are "disordered graphite" and "glassy carbon" (with the exception of two grains with onion morphology that were graphite with a D/G intensity ratio of 0.20), the majority of high-density grains (KFC1) have distinctly better crystalline order (i.e., D/G intensity ratios below 0.5; and are classified as "graphite"). The medium density grains (KFB1) seem to be some sort of a "crossover" fraction, and consist of a mix of "disordered graphite" and "graphite", the latter one being more abundant; in addition, one grain with cauliflower morphology (grain KFB1[0,5]b) has the characteristics of "glassy carbon" with a D/G intensity ratio of 1.26.

Fig. 7 shows differences in morphology and Raman type of individual grains of the three density fractions in more detail. Next to the SEM image of each individual particle its characteristic Raman spectrum is shown; in order to emphasize the differences observed in the D/G intensity ratios, only the spectral region of the 1st-order peaks is plotted (spectral zoom-in from 800 to 2000 Δcm^{-1}). The D/G intensity ratio of each spectrum is listed in Table 1. There is quite obviously a correlation between surface morphology and Raman type. Most KFA1 grains have cauliflower (CF) morphology and have spectra with very intense D peaks that indicate small in-plane crystallite sizes L_a, i.e., very disordered graphite (Fig. 7a). On the other hand, most KFC1 grains have onion (O) morphology and spectra with very small D peaks (Fig. 7c). From the Raman perspective, this must mean that the in-plane crystallite size is substantially increased over that observed in KFA1 grains. According to the historic Tuinstra and Koenig calibration, L_a is at least 10 nm for typical KFC1 grains, and on the order of 3 nm for typical KFA1 grains. As mentioned above, grains from the intermediate density fraction KFB1 are mixed, both in their surface morphology (roughness and overall appearance), and in the type of Raman spectra for the individual grains (Fig. 7b). Some of the grains in the KFB1 fraction with cauliflower morphology can be very disordered graphite (e.g., grains KFB1 [7,3]a and KFB1 [3,7]a), and other grains with onion morphology can be fairly well ordered graphite (e.g., grains KFB1 [5,2]a and KFB1 [6,3]). Several grains with cauliflower–onion (CFO) morphology also have spectra characteristic of well-ordered graphite; for instance, this is the case for grains KFB1 [5,0] and KFB1 [4,7]c. But again, it has to be kept in mind that the morphology classification of "cauliflower–onion" is subjective and many of these grains may have been classified as "onion" types by a different investigator. In other words, the morphology type "cauliflower–onion" has to be taken "with a grain of salt", because it is not unambiguous.

Based on the Raman results shown in Figs. 6 and 7, it is concluded that the Murchison grains essentially fall into two groups as far as the crystallinity of their surfaces is concerned: the KFA1 grains (on average) are distinctly different and are not nearly as well crystallized as the two higher-density fractions. Based on the Raman results, the source and/or thermal history of KFB1 and KFC1 grains was either very similar or even the same. The small differences observed between the averages of the D/G intensity ratios (0.44 ± 0.26 and 0.35 ± 0.26 for KFB1 and KFC1, respectively; see Table 1) could be due to the fact that the KFB1 fraction suffered more from contamination with KFA1 grains than did the KFC1 fraction. However, there are two spectral observations that we made only for some of the grains from the KFC1 fraction: Raman spectra with high fluorescence background and Raman spectra with unusually strong 2nd-order peaks (see discussion below).

Grains of a given morphology type, no matter in which density fractions they occurred, tend to have similar D/G intensity ratios in their Raman spectra. As seen in Fig. 8, there is a strong correlation between Raman type and morphology type, despite the fact that the latter is based on subjective visual descriptions, and the former only measures the degree of crystallinity/order/in-plane crystallite size of the outermost surfaces of the grains.

3.2.2. "*Glassy carbon*"

Spectra with narrow 1st-order peaks, in which the D peak is more intense than the G peak and 2nd-order peaks are weak (Fig. 3c) are very uncommon among the possible spectra for sp^2-bonded carbon. To the authors' knowledge, such spectra have not yet been found in terrestrial natural carbonaceous materials; they do, however, occur for insoluble organic matter (IOM) of the meteorite Allende (Harris et al., 2000; Larsen and Nielsen, 2006; Matsuda et al., 2010) as well as in presolar grains from Orgueil (Wopenka et al., 2011a, 2011b), and are known to occur for synthetically produced samples, which are referred to as "glassy carbon" (Nathan et al., 1974; McCulloch and Prawer, 1995; Escribano et al., 2001; Tao et al., 2011). Glassy carbon is a technologically important material that is known to be

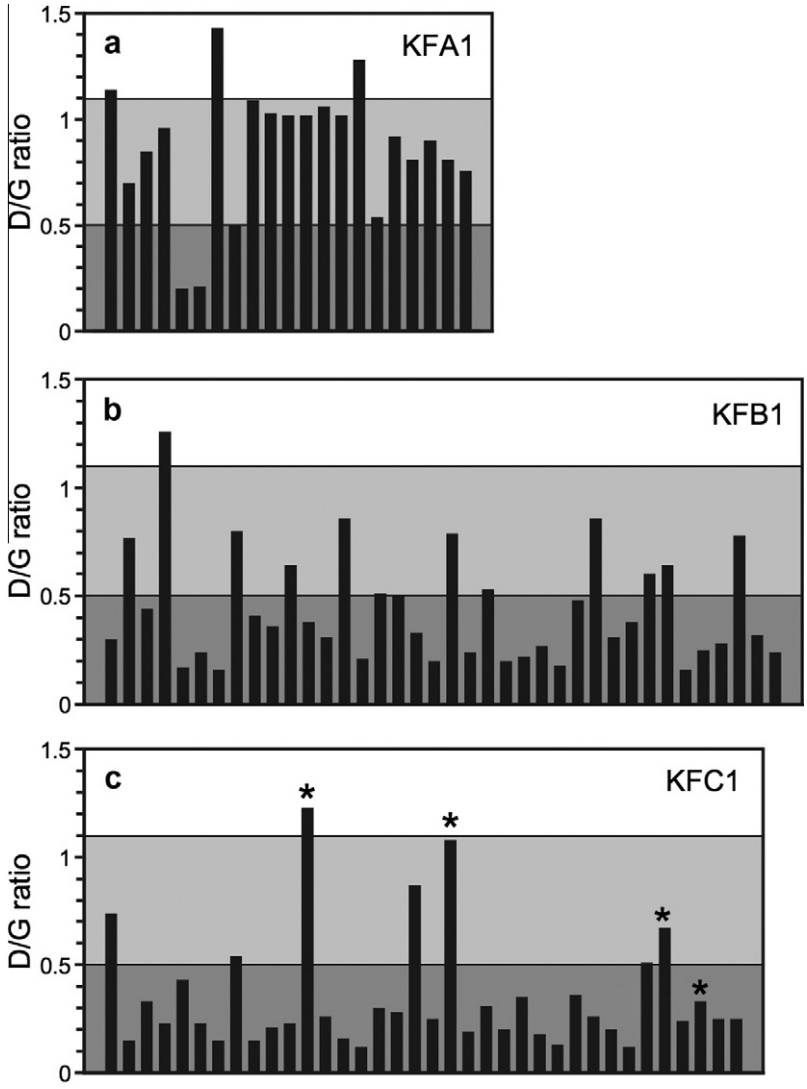

Fig. 6. Raman D/G intensity ratios (Int_D/Int_G; see Fig. 3b) of presolar sp^2-bonded carbon grains from different Murchison separates: low density KFA1, medium density KFB1, and high density KFC1; *x*-axes show the number of grains analyzed in each density fraction. Based on their D/G intensity ratios, the grains were grouped into the following Raman types: (fairly well ordered) "graphite" ($Int_D/Int_G < 0.5$; shaded dark gray), "disordered graphite" ($0.51 < Int_D/Int_G < 1.1$; shaded light gray), and "glassy carbon" ($Int_D/Int_G > 1.1$; white). All three Raman types occur in all three density fractions, but in different abundances. Grains with extremely intense 2nd-order peaks relative to the 1st-order peaks, referred to as "unusual sp^2-bonded carbon", were only found in the high density fraction KFC1, and are marked with an asterisk. Grains with kerogen-type Raman spectra are not included in this figure.

non-graphitizing, i.e., it is a form of carbon which cannot be transformed into crystalline graphite even at temperatures of >3000 °C. It is reported to have extremely weak and broad (100) X-ray diffraction peaks, i.e., it has the diffraction characteristics of an amorphous material. In addition, synthetic glassy carbon is extremely resistant to chemical attack and unaffected by treatment with sulfuric acid and nitric acid (Harris, 2004).

"Glassy carbon" spectra were detected for four Murchison grains from the present study with either cauliflower or cauliflower–onion morphology (Table 1). Two of the glassy carbon spectra of KFA1 grains are compared to the spectrum for Allende IOM in Fig. 9. At first sight, "glassy carbon" Raman spectra look like spectra of disordered graphite, because of their narrow 1st-order bands, i.e., they are very different from the spectra of organic (kerogen-like) carbonaceous material. Their D and G peak widths, however, are slightly increased compared to the ones for disordered graphite, and most notably their 2nd-order peaks, which are related to the three-dimensional ordering of the sp^2-bonded material (e.g., Pimenta et al., 2007; Beyssac and Lazzeri, 2012), are not very intense (compare Fig. 3a and c).

Because of the similarity of their Raman spectra (Fig. 9), we assume that the ordering of the sp^2-bonded carbon sheets in the Allende IOM and in the Murchison glassy carbon grains must be very similar. The HF-HCl acid residue of the Allende meteorite is described to be "turbostratic

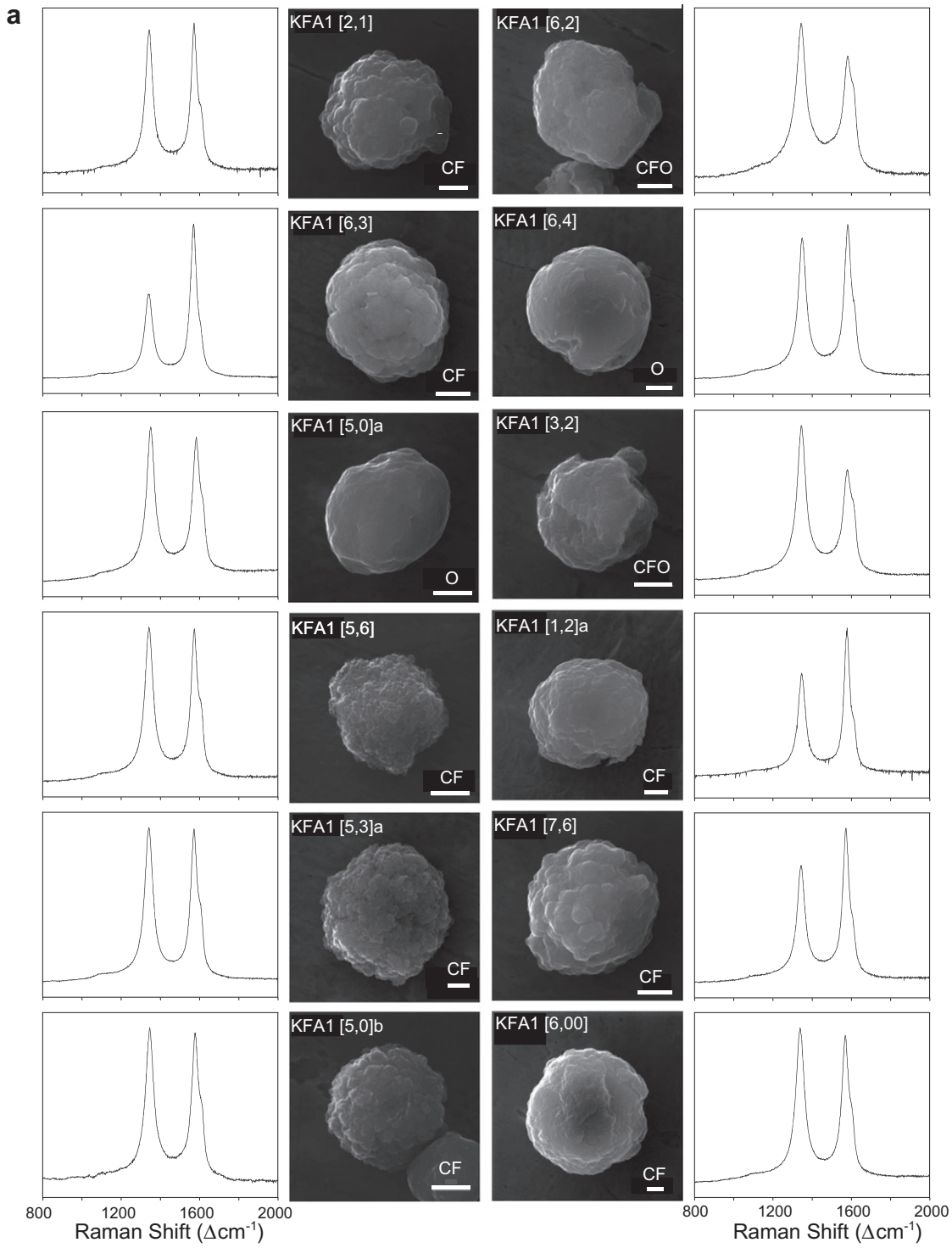

Fig. 7. SEM images (scale bars = 1 μm) and characteristic Raman spectra of 36 typical presolar graphite grains from three different density fractions of the Murchison meteorite. Spectra are plotted as raw spectra (i.e., without baseline correction) with arbitrary intensities on their *y*-axes. The morphology type assigned to each grain is based on these pictures: CF = cauliflower, CFO = cauliflower–onion, O = onion. Raman spectra are plotted from 800–2000 Δcm^{-1}, and thus show only the 1st -order spectrum, in order to emphasize differences in the D/G intensity ratios of grains from different density fractions. Measured D/G peak intensity ratio, Raman type, size, and isotopic ratios are listed in Table 1 in bold font for each grain shown. (a) Grains from low-density fraction KFA1 (2.05–2.10 g/cm^3); average $Int_D/Int_G = 0.87 \pm 0.31$ ($n = 21$); (b) Grains from medium-density fractions KFB1 ((2.10–2.15 g/cm^3); average $Int_D/Int_G = 0.44 \pm 0.26$ ($n = 38$); (c) Grains from high-density fraction KFC1(2.15–2.20 g/cm^3); average $Int_D/Int_G = 0.35 \pm 0.26$ ($n = 36$). The errors given are standard deviations from the mean. Grains with kerogen-type Raman spectra are not included in this figure.

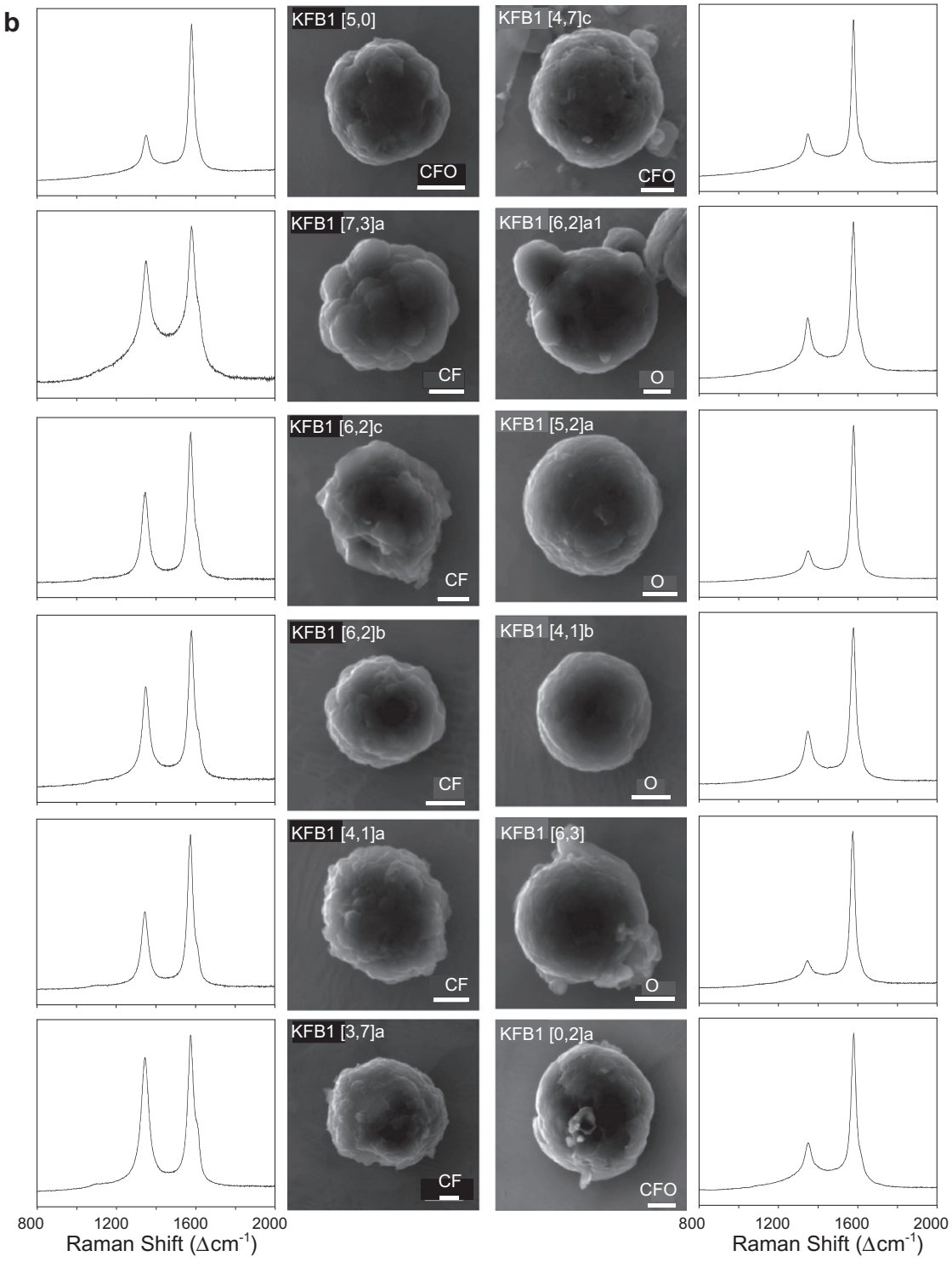

Fig. 7. (*continued*)

carbon" based on TEM observations; lattice fringe images show curved and tangled graphene sheets with *d*-spacings >0.335 nm (Smith and Buseck, 1981; Harris and Vis, 2003; Matsuda et al., 2010). Such "curved and tangled turbostratic carbon" seems to be the same type of material that is called "glassy carbon" in the Raman literature; it does not have any long-range crystalline order in the c-direction, but has very well-defined ordered C–C sp^2-bonds within individual graphene sheets. This situation is nicely reflected in the Raman spectrum for glassy carbon: the first-order peaks (indicative of the in-plane ordering) are very strong and narrow, but the second-order peaks (indicative of the

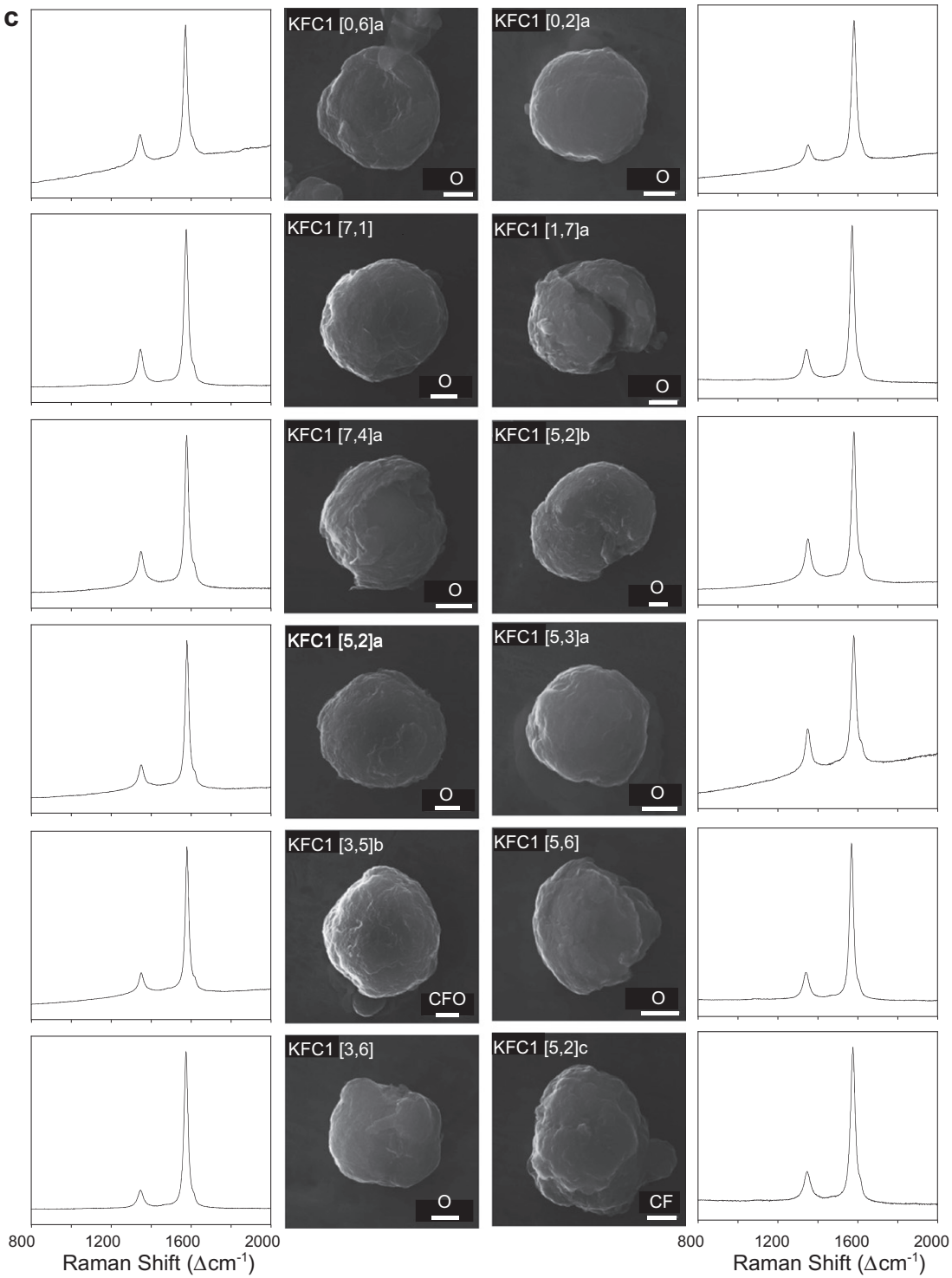

Fig. 7. (*continued*)

ordering along the c-direction) are weak (Fig. 9). This is a very different type of "disorder" than the one referred to as "disordered graphite" or "nanocrystalline graphite", both of which have some long-range/medium-range crystalline order in both L_a and L_c dimensions. The fact that the Raman D and G peaks in glassy carbon are narrow and strong must mean that the sheets are composed of pure carbon (i.e., no heteroatoms like H are present) and that all atoms are being bonded in hexagonal rings (i.e., probably no rings of 5 or 7 carbon atoms exist, contrary to the proposal by Harris, 2004). But since those sheets can be curved (Smith and Buseck, 1981; Harris and Vis, 2003; Croat et al.,

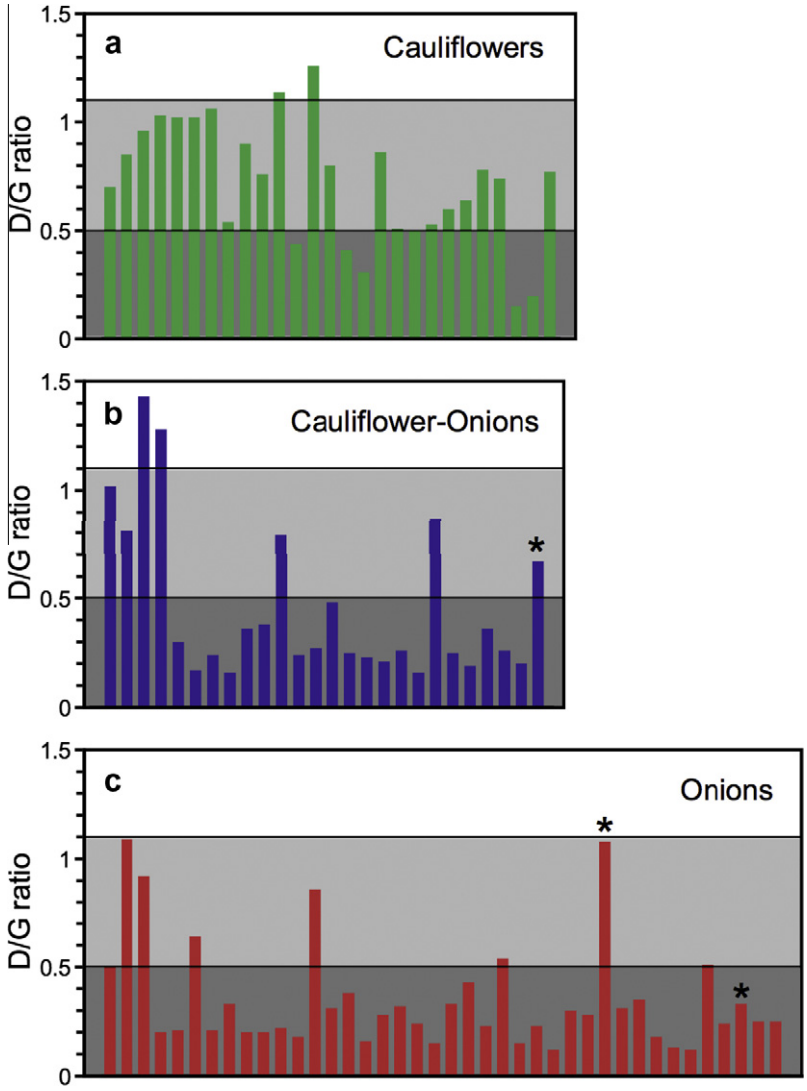

Fig. 8. Raman D/G intensity ratios (Int_D/Int_G; see Fig. 3b) of presolar sp^2-bonded carbon grains that have different surface morphology; *x*-axes show the number of grains analyzed of each morphology type. The density of grains is not indicated, and grains with kerogen-type Raman spectra are not included in this figure. (a) Most grains with cauliflower morphology are "disordered graphite" ($0.51 < Int_D/Int_G < 1.1$; shaded light gray); (b) and (c) Most grains with cauliflower–onion and onion morphology are (are fairly well-ordered) "graphite" ($Int_D/Int_G < 0.5$; shaded dark gray); Grains with a so-called "glassy carbon" Raman spectrum ($Int_D/Int_G > 1.1$; white area) have either cauliflower or cauliflower–onion morphologies; Grains with extremely intense 2nd-order peaks relative to their 1st-order peaks, referred to as "unusual sp^2-bonded carbon", are marked with an asterisk and have either onion or cauliflower–onion morphology.

2008; Matsuda et al., 2010), and since there is no ordering when it comes to the stacking of the sheets, strictly speaking, glassy or turbostratic carbon is amorphous (i.e., "glassy"), and should not be referred to as "nanocrystalline and/or disordered graphite". The 2nd-order Raman spectrum can provide valuable information to clarify whether the material is (disordered) crystalline or amorphous, but unfortunately many of the Raman papers on extraterrestrial carbonaceous materials focus only on the 1st order D and G bands, and fail to report and discuss observations made for the 2nd-order bands (e.g., Busemann et al., 2007; Matsuda et al., 2010). Recently, Stroud et al. (2011) also recognized the presence of glassy carbon (in addition to sp^3-bonded diamond) in acid-resistant nanometer-sized separates from both Allende and Murchison using aberration-corrected scanning transmission electron microscopy with sub-nanometer resolution.

3.2.3. "*Unusual sp^2-bonded carbon*"

Another unusual type of Raman spectrum is obtained from some of the KFC1 grains (Table 1). These spectra tend to have very intense D peaks, and at first sight (especially if one only looks at the 1st-order spectra) appear to be spectra for "glassy carbon" (Fig. 10). However, these spectra are very different from those for "glassy carbon" and "disordered graphite", and thus must be the Raman signatures for "unusual sp^2-bonded carbon". The differences are the following: (1) the 2nd –order peaks of

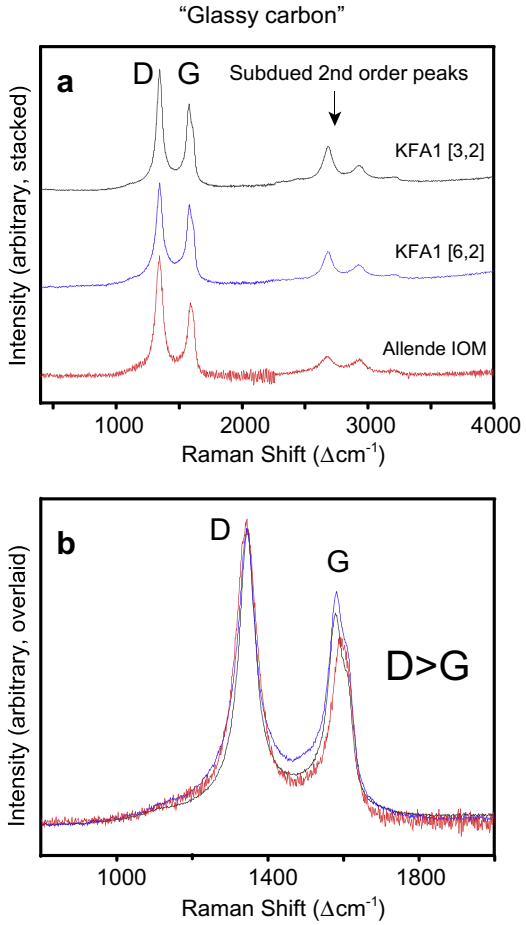

Fig. 9. Raman spectra characteristic of so-called "glassy carbon" ($Int_D/Int_G > 1.1$; subdued 2nd-order peaks). (a) 1st - and 2nd-order spectra (stacked along *y*-axis) obtained for two presolar grains from the Murchison KFA1 low-density fraction are compared to the spectrum for Allende insoluble organic material (IOM; red trace). (b) 1st-order spectra (zoom-in from 800 to 2000 Δcm^{-1}; overlaid on *y* axis) for the same samples to show the spectral similarities among those samples: all spectra have $Int_D > Int_G$, and peak widths for Allende and Murchison KFA1 grains are similar.

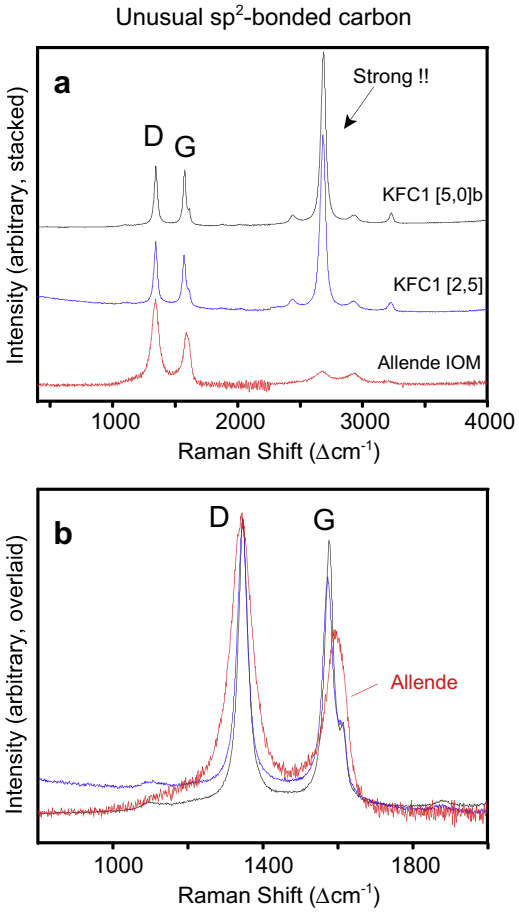

Fig. 10. Raman spectra of unusual sp^2-bonded graphitic carbon obtained for two grains from the Murchison KFC1 high-density fraction are compared to the "glassy carbon" spectrum for Allende's IOM (red trace). (a) 1st- and 2nd-order spectra (stacked along *y*-axis); note the extreme intensity of one of the 2nd-order peaks of the two presolar grains from the Murchison KFC1 high-density fraction compared to the spectrum for Allende IOM (red trace). (b) 1st-order spectra (zoom-in from 800 to 2000 Δcm^{-1}; overlaid on *y* axis) for the same samples show that the peaks for Allende (glassy carbon) are substantial wider than those for the Murchison KFC1 grains. An additional small peak at the right flank of the G peak can be discerned in the spectra of the two KFC1 grains.

the unusual sp^2-bonded carbon are not subdued (like they are in glassy carbon), but rather the opposite: one of the 2nd-order peaks (the one at ~2720 Δcm^{-1}) is extremely intense with respect to the D and G peaks (Fig. 10a; also compare different spectra in Fig. 11); and (2) the D and G peaks for this material are not as wide as they are for glassy carbon or for Allende IOM. Indeed, the peaks in the "unusual sp^2-bonded carbon" grains are so narrow that an additional peak on the high-wavenumber side of the G peak can be resolved as a shoulder (Fig. 10b). This resolved peak at ~1620 Δcm^{-1} is also a disorder-related peak (and is often referred to as D′ peak in the literature; see discussion above), but usually it only can be resolved in well crystalline graphite. Please note that this D′ peak at ~1620 Δcm^{-1} also can be seen in some of the spectra for KFB1 grains and many of the spectra for KFC1 grains (Fig. 7b and c). This well resolved small D′ peak on the high wavenumber side of the G peak is characteristic for graphites with large in-plane crystallite sizes, which indicates that the crystallinity of the graphene sheets of this so-called "unusual sp^2-bonded carbon" must be very good, i.e., its in-plane crystallite size L_a must be rather large. On the other hand, as mentioned above, the 2nd order spectrum is indicative of the crystallographic ordering in the *c*-direction. Thus, the unusually strong peak at 2722 Δcm^{-1} probably means that the stacking of the graphene sheets is unusual in these grains, and this observation might be an indication for the presence of a different graphite polymorph (i.e., one with ABCABC stacking rather than with ABABAB stacking of graphene sheets). The more likely possibility, however, is that this unusual sp^2-bonded carbon is the same kind of material that is described as "platy turbostratic graphite" based on TEM observations of presolar grains (Croat et al., 2003),

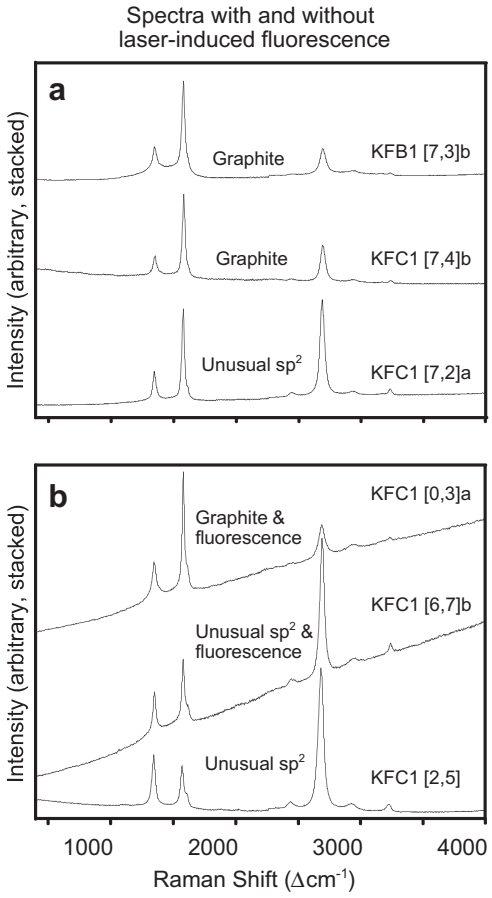

Fig. 11. Raman spectra measured in different presolar sp^2-bonded carbon grain from Murchison with and without laser-induced fluorescence. Fluorescence, which is observed only in grains of the high-density fraction KFC1, occurs in (fairly well) crystallized regular graphite grains as well as in grains with "unusual sp^2-bonded carbon". (a) The spectra of these three grains have no fluorescence, i.e., flat base lines. All three grains have 1st-order peaks indicating well-crystalline graphite, but grain KFC1 [7,2] has a very intense 2nd-order peak and is therefore classified as "unusual sp^2-bonded carbon". (b) Spectra of two grains with fluorescence, resulting in a steeply increasing baseline, and one without fluorescence. The spectrum of grain KFC1 [0,3]a is that of well-crystalline graphite, the spectra of the remaining two grains are those of "unusual sp^2-bonded carbon"; spectra of the latter can have $Int_D < Int_G$ (grain KFC1 [6,7]b) or they can have $Int_D > Int_G$ (grain KFC1 [2,5]); they are classified as "unusual" because of their extremely intense 2nd-order peak at 2722 Δcm^{-1} (see text for discussion).

and referred to as two-dimensional graphene in the materials science literature. Future coordinated TEM and Raman work on individual presolar grains will be needed to clarify this issue.

3.2.4. Laser-induced fluorescence

Laser-induced fluorescence was only observed for about one third of the high-density KFC1 grains (Table 1). Fig. 11 shows examples of grain spectra with and without fluorescence; note that fluorescence only can be observed and documented in raw spectra, and therefore all spectra shown in the present work are presented as raw spectra without any baseline or background correction. Most of the grains with fluorescence are fairly well crystalline graphite grains with either onion or cauliflower–onion morphology, such as grain KFC1 [0,3]a; see Fig. 11b. Two of the grains with fluorescence have high D/G ratios and are classified as disordered graphite (KFC1 [0,1] and KFC1 [6,7]a). In addition, one of the "unusual sp^2-bonded carbon" grains (KFC1 [6,7]b; see Fig. 11b) also shows fluorescence.

Fluorescence can occur when the energy of the visible photons is high enough to induce electronic transitions in the sample. The 532 nm laser excitation used in the present work has sufficient energy to induce transitions between electronic states of organic molecules, i.e., to cause fluorescence. Thus, the collected raw signal is caused by both Raman scattering as well as laser-induced fluorescence. Since the latter is much more intense than the Raman scattering, it can often strongly interfere with the Raman signal. Spectra with fluorescence typically have much lower signal to noise ratios and have the Raman bands superimposed on an intense sloping broad background that increases with increasing relative wavenumbers; this can make it difficult and sometimes even impossible to see the superimposed Raman bands. Specifically, second-order Raman bands from sp^2-bonded carbon can be obscured and/or reduced in relative intensity due to fluorescence. However, whenever fluorescence was observed for graphitic KFC1 grains, it was not very strong, and second-order Raman bands still could be seen.

In Fig. 12 we investigate whether the presence of fluorescence is related to the abundance of nitrogen in the graphitic KFC1 grains. The $^{12}C^{14}N^-/^{12}C^-$ ratio is a measure of the nitrogen content of the grains. Although there is considerable scatter in the plot, on average grains that exhibit fluorescence have higher $^{12}C^{14}N^-/^{12}C^-$ ratios than those without fluorescence. The average $^{12}C^{14}N^-/^{12}C^-$ ratios are 0.14 ± 0.02 (standard error of the mean) for grains with fluorescence and 0.078 ± 0.021 for grains without fluorescence. If we exclude the grain with the largest $^{12}C^{14}N^-/^{12}C^-$ ratio, the later average becomes 0.058 ± 0.010, making the difference even larger. Apparently, fluorescence is related to the N content of the grains. A similar observation has been made about Raman spectra for graphite grains from the Orgueil high-density fraction OR1f (Wopenka et al., 2011b). In agreement with the results on the OR1f grain, also for the Murchison grains we do not find any correlation between fluorescence and any other parameters (i.e., elemental or isotopic compositions) measured in the grains. Of note is that one of the grains with the "unusual sp^2-bonded carbon" (marked with arrows in Fig. 12) also shows fluorescence (grain KFC1 [6,7]b), but the other unusual grains do not (Table 1).

3.2.5. Grains with kerogen-type Raman spectra

A total of eight grains (out of 103) were found to have kerogen-type spectra, and they occurred in all three density fractions (Table 1). Fig. 13 shows both 1st and 2nd-order spectra of two such grains and demonstrates one more time how different kerogen-type spectra are compared to those for very disordered graphite (grain KFA1[5,6]), and quite

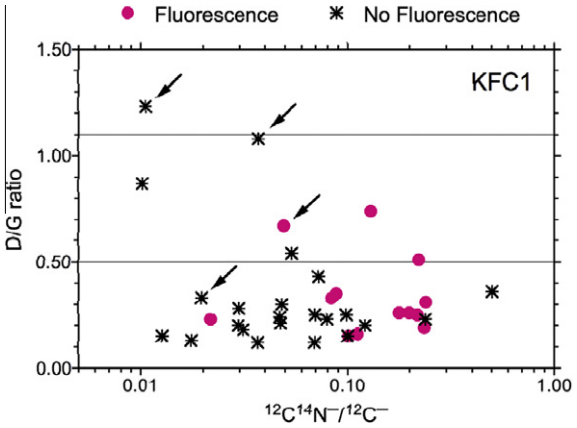

Fig. 12. Raman D/G intensity ratios of high-density graphitic KFC1 grains with and without laser-induced fluorescence are plotted against their $^{12}C^{14}N^{-}/^{12}C^{-}$ ratios. Most grains with fluorescence (plotted as circles) have higher $^{12}C^{14}N^{-}/^{12}C^{-}$ ratios (implying higher N content) than do grains without fluorescence. Arrows point to grains with unusual Raman spectra. See Table 1 for identification of individual grains. Grains with kerogen-type Raman spectra are not included in this figure.

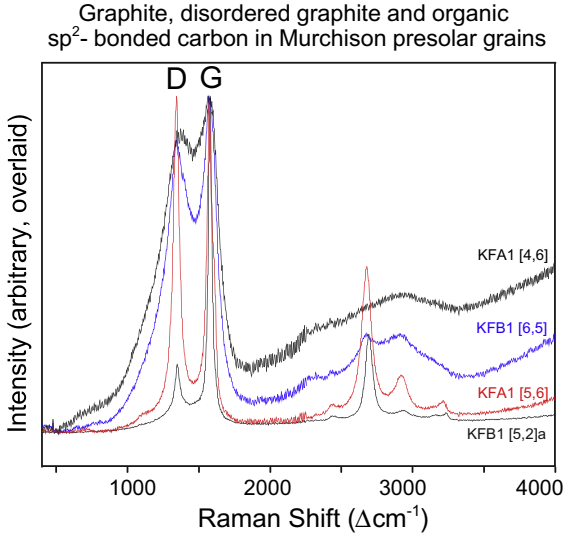

Fig. 13. Raman spectra of grains from Murchison consisting of different types of sp^2-bonded carbon. Grains KFA1 [4,6] and KFB1 [6,5] have kerogen-type spectra with different degrees of fluorescence and almost non-existent or very subdued 2nd-order bands. Kerogen-type spectra are typical for amorphous sp^2-bonded carbon containing heteroatoms, i.e., organic carbonaceous material. In contrast, spectra of ordered and disordered graphite (i.e., inorganic carbon) have very narrow peaks. Grain KFA1 [5,6] has a spectrum with narrow equally strong D and G peaks ($Int_D/Int_G = 1.02$, Table 1) and intense 2nd-order bands and is classified as disordered graphite. Grain KFB1 [5,2]a has the spectrum typical of well-crystalline graphite. All spectra are normalized to the intensity of the G peak.

well ordered graphite (grain KFB1[5,2]a). In general, materials/samples that contain organic carbon and thus yield kerogen-type spectra can often have very strong fluorescence. However, this was not the case for the Murchison grains from the present work; the fluorescence, even though it was there, was not very strong for the 8 kerogen-type spectra, so that the 2nd-order Raman bands still could be seen in some of the spectra (e.g., for grain KFB1[6,5]; Fig. 13).

It did not come as a surprise that the kerogen-type spectra of Murchison presolar grains are different from the characteristic spectrum for the meteorite's matrix (Fig. 14). It is interesting (and was unexpected), however, that the 1st-order kerogen-type spectra of the Murchison grains are all different from one another (Fig. 14). This could indicate that the specific organic molecular make-up for each grain is different and thus the specific organic composition could be characteristic for a given individual grain.

Most grains that have kerogen-type spectra are classified as cauliflower–onions in terms of their morphology/surface appearances (Table 1); upon re-inspection of the SEM pictures, we did not notice any unusual features, and considered it unlikely that the grains were contaminated with "organic crud" from the Murchison matrix. (As a note on the side, many of the presolar carbon grains from Orgueil, especially the ones from the low-density fraction, looked much "dirtier" and had flakes of presumed organic material sticking to their surfaces; Groopman et al., 2012b). Thus, it has to be concluded that the kerogen-type spectra are indigenous to the presolar Murchison grains, rather than caused by surficial contamination. This conclusion is supported by the fact that the C isotopic ratios of all grains with kerogen-type spectra are anomalous; this includes grain KFA1[6,5], for which unfortunately no SEM pictures had been taken.

3.3. Correlation of Raman parameters with isotopic results and astrophysical implications

3.3.1. Grains with narrow Raman peaks: graphite, disordered graphite, glassy carbon and unusual sp^2-bonded carbon

Fig. 15 shows plots of the Raman D/G intensity ratios as function of the $^{12}C/^{13}C$ ratios for the three density fractions of this study. In addition, the data points have different symbols according to their surface morphology. As has been shown above in the histograms (Figs. 6 and 8), on average the Raman D/G ratios depend on both the grains' density and morphology. This Raman result indirectly confirms the strong correlation between the density and the surface morphology of the grains, which has been repeatedly recognized in previous studies of presolar carbon grains (e.g., Hoppe et al., 1995). The distributions of the $^{12}C/^{13}C$ ratios also agree with results of previous studies (Hoppe et al., 1995; Amari et al., 2011): the two higher-density separates KFB1 and KFC1 tend to have larger $^{12}C/^{13}C$ ratios than the low-density KFA1 separate (Fig. 15). A significant fraction of cauliflower grains from KFA1 and a smaller fraction of cauliflower grains from KFB1 have normal $^{12}C/^{13}C$ ratios. The higher density fractions KFB1 and KFC1 contain a few cauliflower grains with high $^{12}C/^{13}C$ ratios, which could be caused by a misidentification of the morphology. As has been observed previously (Hoppe et al., 1995), grains from all density fractions from Murchison can have normal $^{12}C/^{13}C$ ratios, but the relative

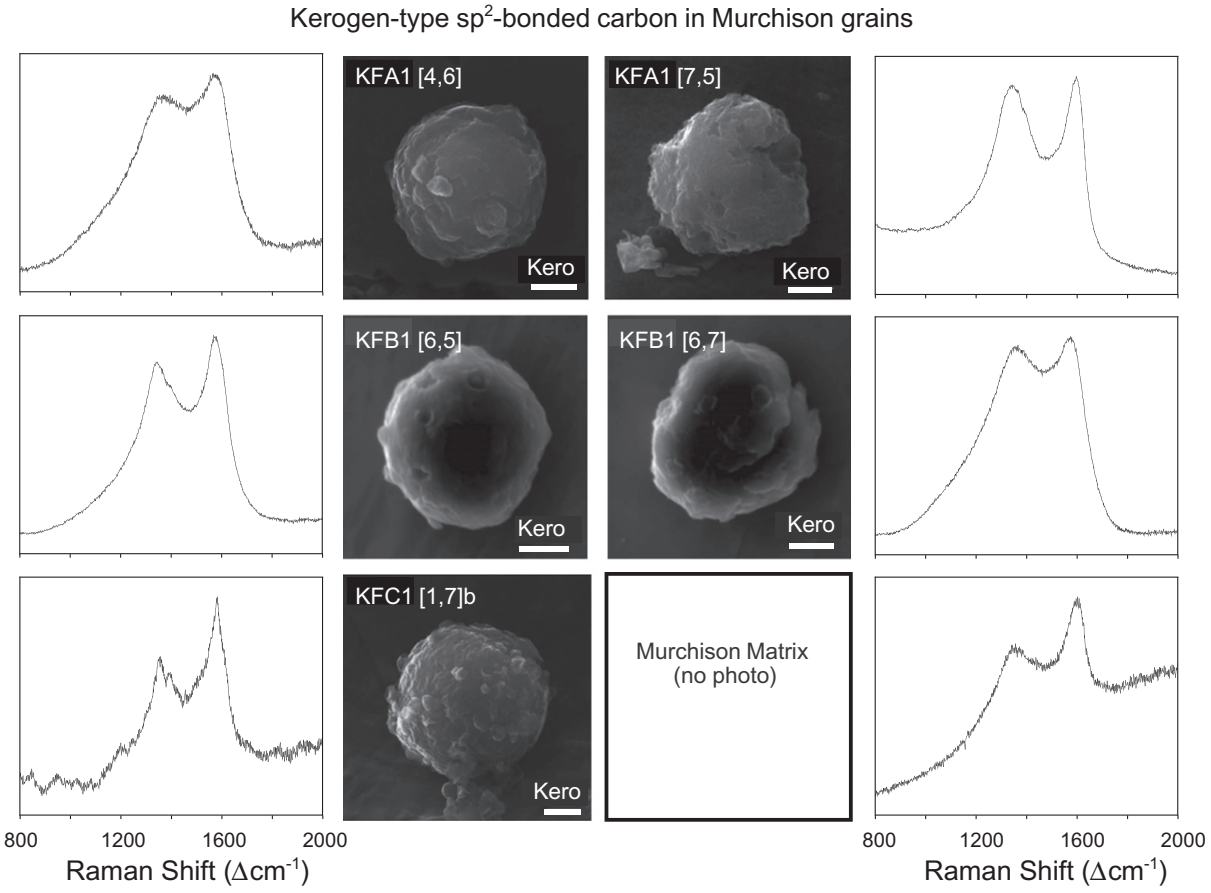

Fig. 14. SEM images (scale bars = 1 μm) and 1st-order Raman spectra of five Murchison presolar "graphite" grains. Spectra are plotted as raw spectra (i.e., without baseline correction) with arbitrary intensities on their *y*-axes. All spectra are so-called "kerogen-type" (i.e., Kero = organic carbon) spectra with very wide D and G peaks and low fluorescence. Each grain has a characteristic Raman spectrum; the spectra for the grains are all different from the one for the meteorite's matrix. The morphology of the grains with kerogen-type spectra is very similar to the morphology of grains with graphitic spectra (see Fig. 7).

percentage of such grains is highest among KFA1, especially for those grains with cauliflower morphology (Fig. 15a), and lowest among KFC1 grains (Fig. 15c). It has been argued that grains with normal $^{12}C/^{13}C$ ratios have a Solar System origin; however this argument cannot be applied to all grains with normal $^{12}C/^{13}C$ ratios; among the KFA1 grains of this study, two cauliflower grains with normal $^{12}C/^{13}C$ ratios (grain KFA1[2,1] and grain KFA1[6,3]) have ^{15}N excesses, indicating an extrasolar origin (Table 1).

We determined the N and O isotopic ratios for all grains of this study (Table 1). The $^{14}N/^{15}N$ and $^{16}O/^{18}O$ are normal (within errors) for most of the grains in the present study, especially for the fractions KFB1 and KFC1. This has been observed previously for density-separated presolar graphite grains, both from Murchison and Orgueil (Zinner et al., 1995; Hoppe et al., 1995; Jadhav et al., 2006, in press). However, grains with highly anomalous $^{12}C/^{13}C$ ratios are expected to also have anomalous $^{14}N/^{15}N$ and $^{16}O/^{18}O$ ratios, whatever their stellar source might be. The reason is that the proton- or alpha-capture reactions, which are the reactions that most strongly affect the C isotopic ratio, also strongly affect the N and O isotopic ratios. This means any H- or He-burning environment would not only produce C but also N and O isotopic anomalies. The fact that the measured N and O isotopic ratios in many presolar graphite grains are normal, despite the fact that the $^{12}C/^{13}C$ ratios are highly anomalous for many of the grains, is a challenge for the interpretation of these results, which has been addressed before. It has been proposed that equilibration and/or contamination with material with normal N and O isotopic ratios is responsible for the unexpected (i.e., normal) N and O isotopic ratios (Hoppe et al., 1995; Zinner, 2007). Such an equilibration and/or contamination obviously would have affected the isotopic ratio of trace elements (N and O) in the carbonaceous material much more heavily than it would have affected the isotopic ratio of the bulk element carbon; thus even though the C isotopic ratios can be anomalous, the N and O isotopic ratios could ended up to be normal. Such a proposed equilibration and/or contamination could have occurred in the Solar Nebula, on the meteorite parent body, or in the laboratory during chemical processing. Because of this problem, N and O isotopic ratios were only of limited usefulness for the identification of presolar grains among graphite grains in previous studies (Hoppe et al., 1995; Jadhav et al., 2006, 2013), as well as in

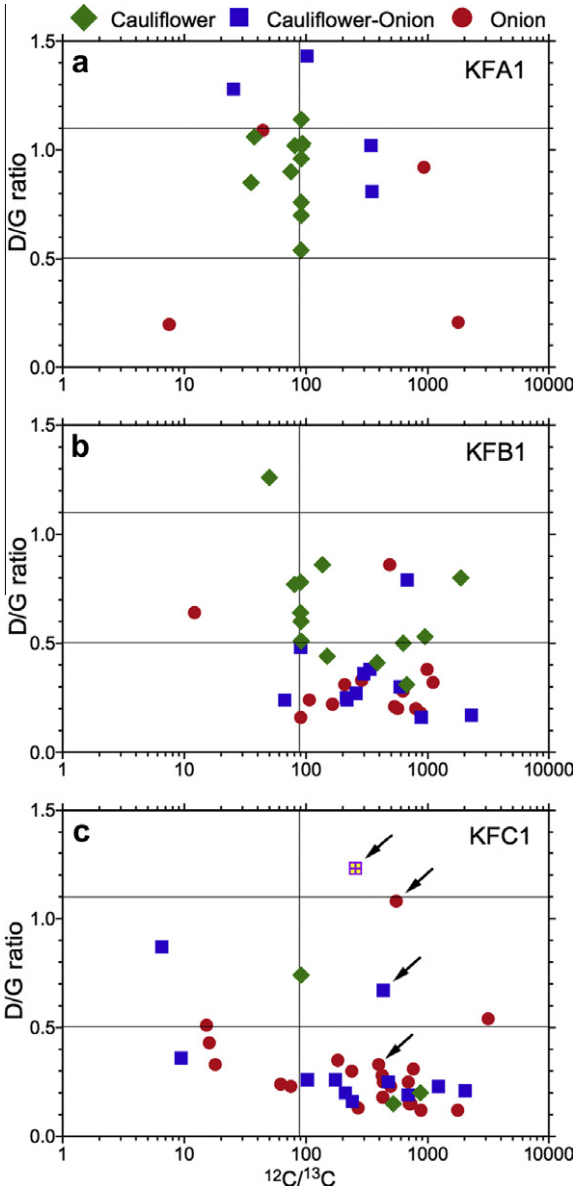

Fig. 15. The Raman D/G intensity ratios (Int_D/Int_G; see Fig. 3) of Murchison grains from three density fractions are plotted against their $^{12}C/^{13}C$ ratios. The data points are labeled according to the surface morphology of the grains. The medium- and high-density grains from the KFB1 and KFC1 fractions tend to have higher $^{12}C/^{13}C$ ratios and lower D/G ratios than the low-density grains from the KFA1 fraction. Arrows in panel c point to grains with "unusual" Raman spectra among the KFC1 density fraction (see text). The one with the highest D/G ratio, grain KFC1[2,5], depicted as a crossed square, has also a morphology different from all the other grains (see Table 1). Grains with kerogen-type Raman spectra are not included in this figure. Solar composition of $^{12}C/^{13}C$ is 89 and indicated with a vertical line.

the present study. Despite this contamination and/or equilibration problem, however, low-density grains seem to better retain their original N and O isotopic signatures than high-density grains (Hoppe et al., 1995; Zinner, 2007; Jadhav et al., 2013), which is also the case for the present study. Of the 24 KFA1 grains listed in Table 1, 14 have excesses in ^{15}N and/or ^{18}O, indicating a supernovae (SN) origin, as has previously been proposed for low-density graphite grains (Hoppe et al., 1995; Travaglio et al., 1999). This includes two grains (KFA1[6,5] and KFA1[7,5]) with kerogen-type Raman spectra, which are not plotted in Fig. 15. All KFB1 grains with normal $^{12}C/^{13}C$ ratios have normal $^{14}N/^{15}N$ and $^{16}O/^{18}O$ ratios but – as mentioned above – because of the equilibration and/or contamination problem afflicting especially high-density grains, we cannot unambiguously assume that all of these grains have a Solar System origin.

It has been proposed that some high-density grains from Orgueil with low $^{12}C/^{13}C$ ratios and very large Ca and Ti isotopic anomalies are from born-again AGB stars (Jadhav et al., 2008). In all three density fractions of the present Murchison study, there are no cauliflower grains with low (<20) $^{12}C/^{13}C$ ratios, but the statistics is limited. Among the five KFC1 grains with low $^{12}C/^{13}C$ ratios (Fig. 15c), three are onions and two are cauliflower–onions; two of these (KFC1[5,00]a and KFC1[5,00]b) have clear ^{15}N excesses and small ^{18}O excesses, and one (KFC1[0,3]c) has a small ^{15}N excess. We do not yet have Ca and Ti isotopic data for the KFC1 grains from the present study, but born-again AGB stars are expected to have high $^{14}N/^{15}N$ ratios rather than ^{15}N excesses. Supernovae can, in principle, produce low $^{12}C/^{13}C$ and low $^{14}N/^{15}N$ ratios (Jadhav et al., 2013), thus it appears that the KFC1 grains with such C and N isotopic signatures from the present study have a SN origin, rather than a born-again AGB star origin. Some high-density grains from Orgueil have been found to exhibit evidence for the initial presence of ^{44}Ti, and thus must also have a SN origin (Jadhav et al., 2013). Among the KFC1 grains, four have unusual Raman spectra with extremely intense 2nd order bands (Table 1; Figs. 10–12). One of them (grain KFC1 [2,5]) also has an unusual shape. All four grains have high $^{12}C/^{13}C$ ratios (Fig. 15c) and have most probably an AGB origin.

3.3.2. Grains with wide Raman peaks: kerogen-type organic carbon

Six of the eight carbon grains with kerogen-type Raman spectra have highly anomalous $^{12}C/^{13}C$ ratios (Table 1). Of note is that the two other grains with close-to-normal ratios (KFA1 [7,5] and KFC1 [1,7]b) had very low secondary ion signals of C during NanoSIMS analysis; furthermore, one of these grains (KFA1 [7,5]) had a very high $^{16}O/^{12}C$ ion ratio (and therefore cannot be a carbon grain), and the other one (grain KFC1 [1,7]b) was not analyzed for N and O; thus, there is the possibility that those two kerogen-type grains were not sp^2-bonded carbon grains, but rather consisted of some other type of organic material. Their $^{12}C/^{13}C$ ratios are normal within large errors.

Of the remaining six kerogen-type grains, three have $^{12}C/^{13}C$ ratios of close to 9. One of them is grain KFC1 [5,00]a, which unfortunately had a very noisy Raman spectrum and therefore was not included in Fig. 14. The remaining three kerogen-type grains have highly anomalous $^{12}C/^{13}C$ ratios of 480, 500, and 990 (Table 1), i.e., there is no doubt that those six grains were formed before our Solar System. In other words, those Murchison grains with the

rather unusual kerogen-type Raman spectra must indeed be presolar carbonaceous grains. The question arises, however, whether the Raman spectra of these grains (shown in Fig. 14) are characteristic for the carbonaceous carrier phase of the isotopic anomalies or whether they are just characteristic for possible contamination with organic carbon on the grains' surfaces. In general, as mentioned above, carbon grains from Murchison were not found to suffer from contamination with adhering IOM material such as it can be the case for presolar grains from Orgueil (Groopman et al., 2012b). Specifically, the SEM images of the Murchison grains from the present study with kerogen-type Raman spectra do not indicate the presence of contamination on their surfaces (Fig. 14).

The possibility of surface contamination with isotopically normal carbonaceous material (IOM or other organic kerogen-like "crud") can be further excluded based on the measurement profiles during isotopic analysis. In the sequence of NanoSIMS measurements of the present study, the first analysis obtained on the Murchison grains was on ^{12}C, ^{13}C, ^{28}Si, ^{29}Si and ^{30}Si simultaneously in multi-detection. During these analyses the primary Cs^+ ion beam is rastered over an area that is typically a little larger than the analyzed grain. Before the start of the isotopic measurement the primary beam is applied to the sample until the negative secondary ion signals indicate equilibrium rates. This is achieved when enough of the sample surface is sputtered away to reach the layer of implanted Cs. The presence of Cs increases negative secondary ion signals by a large factor, which is actually the main reason that Cs^+ is used for the primary beam if negative secondary ions are to be analyzed. Since according to SRIM simulation (Ziegler et al., 2008), the implantation depth of Cs in graphite is 14 nm, we estimate that a layer of about that same thickness was removed before C–Si isotopic analysis started. The analysis for the five isotopes lasted for ~220 s, with 200 s spent on ion counting, and ~20 s needed for peak centering. Fig. 16 shows profiles of $^{12}C/^{13}C$ ratios measured in the six isotopically anomalous grains with kerogen-type Raman spectra as function of analysis time. It can be seen that, except for fluctuations because of counting statistics, the measured ratios are perfectly constant throughout the analysis. If there were contamination with isotopically normal C on the surface (which would be the reason for the observed kerogen-type Raman spectra of these six grains), this contamination would had to be thinner than 14 nm, and even then we would expect to see an effect at the beginning of the analyses because of atomic knock-on mixing by the primary ion beam. From the total number of detected C ions we can estimate the thickness of the layer removed during the analysis. If we assume an useful ion yield (detected ions per sputtered atoms) of 1% for C (probably a lower limit), we derive thicknesses between 5 and 15 nm for five grains (we do not know the size of grain KFA1 [6,5]). As mentioned above, Raman spectroscopy is a surface technique for opaque samples, and only at most the top ~100 nm of the sample are analyzed (for 532 nm excitation). This Raman-analyzed thickness is approximately commensurate with the thickness probed by the C–Si isotopic analyses: a NanoSIMS measurement time profile of

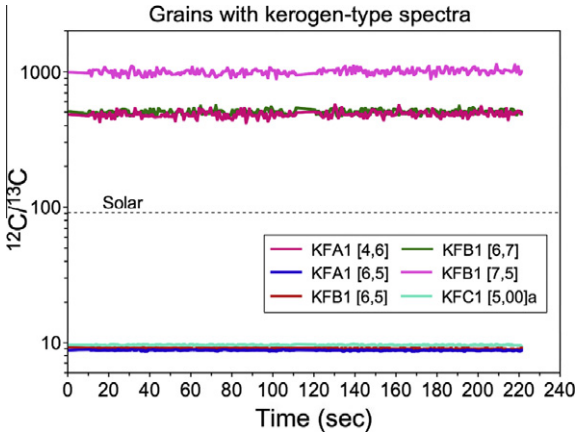

Fig. 16. Profiles of the $^{12}C/^{13}C$ ratios of six grains with kerogen-type Raman spectra during isotopic NanoSIMS measurements as a function of analysis time (and depth). All six grains have extremely anomalous isotopic ratios (see Table 1). The perfectly constant ratios of all grains during analysis indicate the lack of contamination with carbonaceous material with isotopically normal organic C at the surface of the grains, and support the conclusion that the kerogen-type (i.e., organic) carbon is indeed presolar in origin and the carrier phase for the isotopic anomalies.

200 s corresponds to a depth profile of ~15 nm. Thus, we conclude that the carrier phases for the isotopic carbon anomalies in these grains is indeed some form of organic carbon that is reflected in a 'kerogen-type" Raman spectrum.

In order to investigate whether grains with kerogen-type spectra have higher concentrations of N and O, we plotted the ion ratios of $^{12}C^{14}N$ and ^{16}O relative to ^{12}C against one another (Fig. 17). As can be seen, these ratios for the kerogen-type grains (shown in filled symbols in Fig. 17) are not unusual or systematically higher than those for the other (i.e., graphitic or glassy carbon) grains. Kerogen-type grains probably have higher hydrogen contents than the other grains, but hydrogen was unfortunately not measured in the grains of the present study. Messenger et al. (1998) detected polycyclic aromatic hydrocarbons (PAHs) by two-step laser desorption laser ionization mass spectrometry (μL^2MS) in presolar graphite grains from Murchison with a large range in $^{12}C/^{13}C$ ratios. PAH concentrations ranged up to 5000 ppm. The authors argued that the PAHs are indigenous, in particular for grains with C isotopic anomalies in their molecular mass spectra. Unfortunately, no information exists about the molecular/crystalline structure of the grains analyzed by μL^2MS, but a mixture of large PAHs would indeed have a kerogen-type Raman spectrum with very wide peaks.

It is peculiar that the kerogen-type grains can have such extreme $^{12}C/^{13}C$ ratios in both directions (either very low or very high $^{12}C/^{13}C$; see Table 1). Two of the grains (KFA1 [6,5] and KFC1 [5,00]a) with low $^{12}C/^{13}C$ ratios have ^{15}N excesses, indicating a SN origin. The 25 $M_\odot$ SN model by Rauscher et al. (2002) and a series of SN models by A. Heger with masses from 24 to 40 $M_\odot$ (http://webusers.physics.umn.edu/~alex/sollo03/) feature a ^{15}N spike in the He/N zone where $^{12}C/^{13}C$ ratios are as low as 3.5. The isotopic

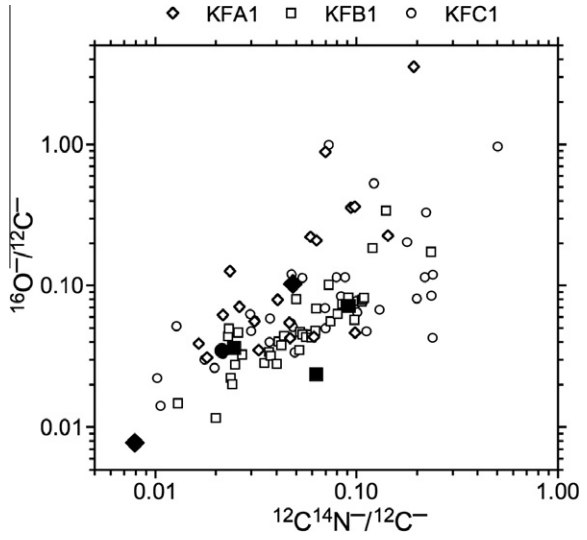

Fig. 17. Ion ratios $^{16}O/^{12}C$ are plotted against ion ratios $^{12}C^{14}N/^{12}C$ for all 103 carbon grains of this study. Data points are labeled according to the density fractions of the grains. Grains with kerogen-type Raman spectra are indicated by filled symbols. It can be seen that the kerogen-type grains do not have any higher N and O contents than the graphitic grains. Thus, it is assumed that the kerogen-type Raman spectra observed for these grains is mostly caused by a high hydrogen content.

ratios of the three kerogen-type grains with $^{12}C/^{13}C$ of ~9 (see Table 1) can, at least according to the theoretical models, be reproduced by such supernovae. The isotopic signatures (i.e., $^{12}C/^{13}C$ of ~9) would exclude AGB stars as the sources of these grains. In particular, models of AGB stars for a large range of masses and metallicites indicate that $^{12}C/^{13}C$ ratios on the surface of the stars are much larger than 10 when C > O, the condition for the condensation of graphite (Zinner et al., 2006b). It is more difficult to identify and suggest stellar sources for the three kerogen-type grains with high $^{12}C/^{13}C$ ratios (up to ~1000; see Table 1) because of the absence of any diagnostic isotopic signature in the N and O isotopic ratios. In principle, both supernovae and low-metallicity AGB star can produce high $^{12}C/^{13}C$ ratios; in the first case one expects low $^{14}N/^{15}N$ and low $^{16}O/^{18}O$ ratios, in the second case the opposite. It would simplify the picture if we could prove that all kerogen-type grains have a SN origin, but at the present time we are not able to make this claim with any confidence and we have to wait for more conclusive evidence.

4. CONCLUDING REMARKS

We have shown that Raman spectroscopy is a useful tool for the structural characterization of presolar graphite grains. The only other technique that can give information about the degree of (nano)crystallinity and/or the amorphous character of individual presolar carbon grains is TEM. The latter, however, requires a much more elaborate sample preparation, and is substantially more time-consuming and complicated than Raman microprobe spectroscopy. In contrast to the detailed information that can be obtained from both the outside and the inside of a grain via TEM, the Raman spectrum of an opaque whole grain (to study the interior of grains by TEM one has to slice the grain; Raman analysis can also be made on slices) can only give information about the ordering/crystallinity of its top 100 nm surface. In the case of presolar grains, however, the crystallinity of this surface seems to be a representative parameter for a given grain. Raman spectra obtained on individual μm-sized spots of 103 grains have shown that (1) each grain has a characteristic type of Raman spectrum that is the same for different spots analyzed on the surface of a given grain, (2) grains from the low density fraction KFA1 tend to have smaller in-plane crystallite sizes of sp^2-bonded carbon than grains from the two higher-density fractions KFB1 and KFC1, (3) there exists a strong correlation between Raman spectral parameters (i.e., D/G intensity ratios) and the surface morphology of individual graphitic grains, (4) so-called "glassy carbon" only occurs in low- and medium density grains, (5) laser-induced fluorescence only occurs in high-density grains and is correlated with the amount of nitrogen in the sample, (6) unsually strong second-order peaks only occur in high-density grains, and (7) grains with organic kerogen-type sp^2-bonded Raman spectra are rare, but occur in all three density fractions.

For the present study, the isotopic findings on most of the grains have added nothing new to our previous knowledge about presolar carbon grains. As was reported in earlier SIMS studies (Hoppe et al., 1995), we also found (1) that the KFB1 and KFC1 grains have larger $^{12}C/^{13}C$ ratios than do the low-density KFA1 grains (Fig. 15), and (2) that despite their anomalous carbon isotopic ratios, most KFB1 and KFC1 grains have isotopically normal nitrogen and oxygen. To find normal N and O in grains with anomalous C isotopic ratios is unexpected; this only can be explained and "blamed" on contamination and/or equilibration, and has been done so in the past (Hoppe et al., 1995; Jadhav et al., 2006, 2013).

The crystalline structure of presolar graphite grains as revealed by Raman spectroscopy is in general agreement with expectation of their origin in AGB stars and supernovae. We have seen that on average low-density grains from the KFA1 separate have higher Raman D/G ratios than medium- and high-density grains from the separates KFB1 and KFC1, indicating a more disturbed structure. This means that low-density grains, which are believed to have a SN origin, are less well crystallized than high-density grains, most of which probably come from AGB stars. It is not unexpected that SN grains, which condense from turbulent ejecta (e.g., Hammer et al., 2010) in a relatively short time have a more disordered structure than grains from AGB stars, which condense from less turbulent stellar winds during a longer time period, which can be as large as a few years (Bernatowicz et al., 2005). An interesting finding is that two KFC1 grains whose C and N isotopic ratios indicate a SN origin (grains [5,00]a and [5,00]b) also have Raman spectra that are atypical for KFC1 grains: one grain ([5,00]b) has a high D/G ratio, whereas the other grain ([5,00]a) has a kerogen-type Raman spectrum (Table 1). Such correlations between isotopic data and

Raman spectra of individual grains help to (1) confirm the hypotheses that carbon grains come from different types of stellar sources, and (2) show that the density separations are probably not perfect and that individual grains with low-density can cross over into one of the higher-density fractions and vice versa. This cross-over effect is especially obvious for the medium-density KFB1 separate, which indeed seems to be a mixture of low-density KFA1grains and high-density KFC1 grains; the latter is indicated by the grains' morphology (Fig. 4), their Raman D/G ratios (Fig. 6), as well as their carbon isotopic ratios (Fig. 15).

The results of the present Raman study for Murchison grains echo our previous Raman results for presolar carbon grains isolated from Orgueil. Also for Orgueil, (1) so-called "glassy carbon" was only found among the low-density grains (Wopenka et al., 2011a), (2) sp^2-bonded graphitic carbon of much better (but variable) crystallinity/ordering was found for most of the high-density grains (Wopenka et al., 2011b), (3) some of the high-density grains were found to have laser-induced fluorescence (which correlates with the nitrogen contents of the grains, just as is the case for the Murchison grains), and (4) few grains were found to have kerogen-type spectra. The latter, however, in the case of Orgueil grains was mostly blamed on contamination with organic carbon ("crud") coming from the IOM that could not be eliminated (Groopman et al., 2012b). (It was difficult to isolate clean presolar grains from Orgueil, because the remaining IOM stubbornly "stuck" to the grains' surfaces.) Based on the results of the present coordinated Raman-NanoSIMS study, however, we conclude that the carrier phases for the carbon isotopic anomalies in some of the Murchison grains is indeed some form of organic carbonaceous material. In summary, sp^2-bonded carbon found in presolar meteorite grains ain't always graphite: some of it is amorphous and can be described as glassy inorganic carbon, and some of it is amorphous and can be described as or organic or "kerogen-like" carbon.

ACKNOWLEDGMENTS

We thank Frank Gyngard and Tim Smolar for keeping the NanoSIMS and its users happy, and Peter Hoppe for being a very meticulous reviewer. This work was supported by NASA Grants NNX10AI45G (T. Bernatowicz, PI) and NNX11AH14G (E. Zinner, PI).

REFERENCES

Allamandola L. J., Sandford S. A. and Wopenka B. (1987) Interstellar polycyclic aromatic hydrocarbons and the carbon in interplanetary dust particles and meteorites. *Science* **237**, 56–59.

Amari S., Anders E., Virag A. and Zinner E. (1990) Interstellar graphite in meteorites. *Nature* **345**, 238–240.

Amari S., Hoppe P., Zinner E. and Lewis R. S. (1993) The isotopic compositions and stellar sources of meteoritic graphite grains. *Nature* **365**, 806–809.

Amari S., Lewis R. S. and Anders E. (1994) Interstellar grains in meteorites: I. Isolation of SiC, graphite, and diamond; size distributions of SiC and graphite. *Geochim. Cosmochim. Acta* **58**, 459–470.

Amari S., Lewis R. S. and Anders E. (1995a) Interstellar grains in meteorites: III. Graphite and its noble gases. *Geochim. Cosmochim. Acta* **59**, 1411–1426.

Amari S., Zinner E. and Lewis R. S. (1995b) Large ^{18}O excesses in circumstellar graphite grains from the Murchison meteorite: indication of a massive star-origin. *Astrophys. J.* **447**, L147–L150.

Amari S., Zinner E. and Lewis R. S. (1996) ^{41}Ca in presolar graphite of supernova origin. *Astrophys. J.* **470**, L101–L104.

Amari S., Zinner E., Gallino R. and Lewis R. S. (2011) Presolar graphite from Murchison. *Lunar Planet Sci.* ***XLII***. #1098 (abstr.).

Beny-Bassez C. and Rouzaud J. N. (1985) Characterization of carbonaceous materials by correlated electron and optical microscopy and Raman microspectroscopy. *Scan. Electron Microsc.* **1985**, 119–132.

Bernatowicz T. J., Amari S., Zinner E. K. and Lewis R. S. (1991) Interstellar grains within interstellar grains. *Astrophys. J.* **373**, L73–L76.

Bernatowicz T. J., Cowsik R., Gibbons P. C., Lodders K., Fegley, , B., Amari S. and Lewis R. S. (1996) Constraints on stellar grain formation from presolar graphite in the Murchison meteorite. *Astrophys. J.* **472**, 760–782.

Bernatowicz T. J., Akande O. W., Croat T. K. and Cowsik R. (2005) Constraints on grain formation around carbon stars from laboratory studies of presolar graphite. *Astrophys. J.* **631**, 988–1000.

Beyssac O., Goffé B., Chopin C. and Rouzaud J.-N. (2002) Raman spectra of carbonaceous material in metasediments: a new geothermometer. *J. Metamorph. Geol.* **20**, 859–871.

Beyssac O. and Lazzeri M. (2012) Application of Raman spectroscopy to the study of graphitic carbons in the Earth Sciences. European Mineralogical Unions (EMU). *Notes Mineral.* **12**, 413–452, Chapter 12.

Bonal L., Quirico E., Bourot-Denise M. and Montagnac G. (2006) Determination of the petrologic type of CV3 chondrites by Raman spectrscopy of included organic matter. *Geochim. Cosmochim. Acta* **70**, 1849–1863.

Bonal L., Bourot-Denise M., Quirico E., Montagnac G. and Lewin E. (2007) Organic matter and metamorphic history of CO chondrites. *Geochim. Cosmochim. Acta* **71**, 1605–1623.

Busemann H., Alexander C. M. O. D. and Nittler L. R. (2007) Characterization of insoluble organic matter in primitive meteorites by microRaman spectroscopy. *Meteorit. Planet. Sci.* **37**, 1387–1416.

Croat T. K., Bernatowicz T., Amari S., Messenger S. and Stadermann F. J. (2003) Structural, chemical, and isotopic microanalytical investigations of graphite from supernovae. *Geochim. Cosmochim. Acta* **67**, 4705–4725.

Croat T. K., Stadermann F. J. and Bernatowicz T. J. (2005) Presolar graphite from AGB stars: microstructure and s-process enrichment. *Astrophys. J.* **631**, 976–987.

Croat T. K., Stadermann F. and Bernatowicz T. (2008) Correlated isotopic and microstructural studies of turbostratic presolar graphites from the Murchison meteorite. *Meteorit. Planet. Sci.* **43**, 1497–1516.

Croat T. K., Stadermann F. J. and Bernatowicz T. J. (2010) Unusual $^{29,30}Si$-rich SiCs of massive star origin found within graphite from the Murchison meteorite. *Astron. J.* **139**, 2159–2169.

Dobrica E., Engrand C., Quirico E., Montagnac G. and Duprat J. (2011) Raman characterization of carbonaceous matter in CONCORDIA Antarctic micrometeorites. *Meteorit. Planet. Sci.* **46**, 1363–1375.

Dresselhaus M. S., Dresselhaus G., Pimenta M. A. and Eklund P. C. (1999) Raman scattering in carbon materials. In *Analytical*

Applications of Raman Spectroscopy (ed. M. J. Pelletier). Blackwell Publishing, 496.

Dresselhaus M. S., Jorio A., Hofmann M., Dresselhaus G. and Saito R. (2010) Perspectives on carbon nanotubes and graphene Raman spectroscopy. *Nanoletters* **20**, 751–758.

Escribano R., Sloan J. J., Siddique N., Sze N. and Dudev T. (2001) Raman spectroscopy of carbon-containing particles. *Vib. Spectrosc.* **26**, 179–186.

Ferrari A. C. (2007) Raman spectroscopy of graphene and graphite: disorder, electron – phonon coupling, doping and nonadiabatic effects. *Solid State Commun.* **143**, 47–57.

Ferrari A. C. and Robertson J. (2000) Interpretation of Raman spectra of disordered and amorphous carbon. *Phys. Rev. B* **61**, 14095–14107.

Ferrari A. C., Meyer J. C., Scardaci V., Casiraghi C., Lazzeri M., Mauri F., Picanec S., Jiang D., Novoselov K. S., Roth S. and Geim A. K. (2006) Raman spectrum of graphene and graphene layers. *Phys. Rev. Lett.* **97**, 187401–187404.

Grew E. S. (1974) Carbonaceous material in some metamorphic rocks of New England and other areas. *J. Geol.* **82**, 50–73.

Groopman E., Wopenka B., Bernatowicz T. and Zinner E. (2012a) Heterogeneous distributions of C, N, and O isotopes and Raman signatures in low-density supernova graphite grains from Orgueil. *Lunar Planet. Sci. XLIII*. #2126 (abstr.).

Groopman E., Bernatowicz T. and Zinner E. (2012b) C, N, and O isotopic heterogeneities in low-density supernova graphite grains from Orgueil. Astrophys. J. **754**, L8 (6pp).

Hammer N. J., Janka H.-T. and Müller E. (2010) Three-dimensional simulations of mixing instabilities in supernova explosions. *Astrophys. J.* **714**, 1371–1385.

Harris P. J. F. (2004) Fullerene-related structure of commercial glassy carbons. *Philos. Mag.* **84**, 3159–3167.

Harris P. J. F. and Vis R. D. (2003) High-resolution transmission electron microscopy of carbon and nanocrystals in the Allende meteorite. *Proc. R. Soc. Lond.* **459**, 2069–2076.

Harris P. J. F., Vis R. D. and Heymann D. (2000) Fullerene-like carbon nanostructures in the Allende meteorite. *Earth Planet. Sci. Lett.* **183**, 355–359.

Heck P. R., Amari S., Hoppe P., Baur H., Lewis R. S. and Wieler R. (2009) Ne isotopes in individual presolar graphite grains from the Murchison meteorite together with He, C, O, Mg–Al isotopic analyses as tracers of their origins. *Astrophys. J.* **701**, 1415–1425.

Hoppe P., Amari S., Zinner E. and Lewis R. S. (1995) Isotopic compositions of C, N, O, Mg, and Si, trace element abundances, and morphologies of single circumstellar graphite grains in four density fractions from the Murchison meteorite. *Geochim. Cosmochim. Acta* **59**, 4029–4056.

Hynes K. M. and Gyngard F. (2009) The presolar grain database: http://presolar.wustl.edu/~pgd. *Lunar Planet. Sci. XL*, #1198 (abstr.).

Jadhav M., Amari S., Zinner E. and Maruoka T. (2006) Isotopic analysis of presolar graphite grains from Orgueil. *New Astron. Rev.* **50**, 591–595.

Jadhav M., Amari S., Marhas K. K., Zinner E., Maruoka T. and Gallino R. (2008) New stellar sources for high-density, presolar graphite grains. *Astrophys. J.* **682**, 1479–1485.

Jadhav M., Wopenka B., Amari S., Maruoka T. and Zinner E. (2010) High-density, carbon-13 enriched graphite grains from Orgueil. *Meteorit. Planet. Sci.* **45**, A9.

Jadhav M., Amari S., Zinner E., Maruoka T., Marhas K. K. and Gallino R. (2013) Multi-element isotopic analyses of presolar graphite grains from Orgueil. *Geochim. Cosmochim. Acta*.

Jadhav M., Savina M. R., Jokela S., Elam J., Huss G. R. and Zinner E. (2012) Zr and Ba isotopic compositions of high-density graphite grains from Orgueil. *Meteorit. Planet. Sci.* **47**, #5183.

Larsen K. L. and Nielsen O. F. (2006) Micro-Raman spectroscopic investigations of graphite in the carbonaceous meteorites Allende, Axtell and Murchison. *J. Raman Spectrosc.* **37**, 217–222.

Lespade P., Marchand A., Couzi M. and Cruege F. (1984) Characterization of carbon materials with Raman microspectrometry. *Carbon* **22**, 375–385.

Lucchese M. M., Stavale F., Martins Ferreira E. H., Vilani C., Moutinho M. V. O., Capaz R. B., Achete C. A. and Jorio A. (2010) Quantifying ion-induced defects and Raman relaxation length in graphene. *Carbon* **48**, 1592–1597.

Matsuda J., Morishita K., Tsukamoto H., Miyakawa C., Nara M., Amari S., Uchiyama T. and Takeda S. (2010) An attempt to characterize phase Q: noble gas, Raman spectroscopy and transmission electron microscopy in residues prepared from the Allende meteorite. *Geochim. Cosmochim. Acta* **74**, 5398–5409.

McCulloch D. G. and Prawer S. (1995) The effect of annealing and implantation temperature on the structure of C ion-beam-irradiated glassy carbon. *J. Appl. Phys.* **78**, 3040–3047.

McFeely F. R., Kowalczyk S. P., Ley L., Cavell R. G., Pollak R. A. and Shirley D. A. (1974) X-ray photoemission studies of diamond, graphite, and glassy carbon valence bands. *Phys. Rev. B* **9**, 5268–5278.

Meier M. M. M., Heck P. R., Amari S., Baur H. and Wieler R. (2012) Graphite grains in supernova ejecta – insights from a noble gas study of 91 individual KFC1 presolar graphite grains from the Murchison meteorite. *Geochem. Cosmochim. Acta* **76**, 147–160.

Messenger S., Amari S., Gao X., Walker R. M., Clemett S., Chillier X. D. F., Zare R. N. and Lewis R. (1998) Indigenous polycyclic aromatic hydrocarbons in circumstellar graphite grains from primitive meteorites. *Astrophys. J.* **502**, 284–295.

Mildner D. F. R. and Carpenter J. M. (1982) On the short range atomic structure of non-crystalline carbon. *J. Non-Crystal. Solids* **47**, 391–402.

Nakamizo M., Kammereck R. and Walker, Jr., P. L. (1974) Laser Raman studies on carbons. *Carbon* **12**, 259–267.

Nathan M. I., Smith J. E. and Tu K. N. (1974) Raman spectra of glassy carbon. *J. Appl. Phys.* **45**, 2370.

Nichols, Jr., R. H., Kehm K. and Hohenberg C. M. (1995) Microanalytical laser extraction of noble gases: techniques and applications. In *Advances in Analytical Geochemistry*, vol. 2 (eds. M. Hyman and M. Rowe). JAI Press Inc., pp. 119–140.

Nicolussi G. K., Pellin M. J., Davis A. M., Lewis R. S. and Clayton R. N. (1998) Zr and Mo isotopes in single presolar graphite grains: a record of stellar nucleosynthesis. *Lunar Planet. Sci. XXIX*. #1415 (abstr.).

Nittler L. R., Amari S., Zinner E., Woosley S. E. and Lewis R. S. (1996) Extinct ^{44}Ti in presolar graphite and SiC: proof of a supernova origin. *Astrophys. J.* **462**, L31–L34.

Piani L., Robert F., Beyssac O., Binet L., Bourot-Denise M., Derenne S., Guillou C., Marrocchi Y., Mostefaoui S., Rouzaud J.-N. and Thomen A. (2012) Structure, composition, and location of organic matter in the enstatite chondrite Sahara 97096 (EH3). *Meteorit. Planet. Sci.* **47**, 8–29.

Pimenta M. A., Dresselhaus G., Dresselhaus M. S. and Cancado L. G. (2007) Studying disorder in graphite-based systems by Raman spectroscopy. *Phys. Chem. Chem. Phys.* **9**, 1276–1291.

Quirico E., Rouzaud J. N., Bonal L. and Montagnac G. (2005a) Maturation grade of coals as revealed by Raman spectroscopy: progress and problems. *Spectrochim. Acta A* **61**, 2368–2377.

Quirico E., Borg J., Raynal P.-I., Montagnac G. and d'Hendecourt L. (2005b) A micro-Raman study of 10 IDPs and 6 carbonaceous chondrites. *Planet. Space Sci.* **53**, 1443–1448.

Rauscher T., Heger A., Hoffman R. D. and Woosley S. E. (2002) Nucleosynthesis in massive stars with improved nuclear and stellar physics. *Astrophys. J.* **576**, 323–348.

Reich S. and Thomsen C. (2004) Raman spectroscopy of graphite. *Philos. Trans. R. Soc. Lond. A* **362**, 2271–2288.

Rotundi A., Baratta G. A., Borg J., Brucato J. R., Busemann H., Colangeli L., d'Hendecourt L., Djouadi Z., Ferrini G., Franchi I. A., Fries M., Grossemy F., Keller L.P., Mennella V., Nakamura K., Nittler L.R., Palumbo M.E., Sandford S.A., F. J., Steele A. and Wopenka B. (2008) Combined micro-Raman, micro-infrared, and filed emission scanning electron microscope analyses of Comet 81P/Wild 2 particles collected by Stardust. *Meteorit. Planet. Sci.* **43**, 367–397.

Schopf J. W., Kudryavtsev A. B., Agresti D. G., Wdowiak T. J. and Czaja A. D. (2002) Laser-Raman imagery of Earth's earliest fossils. *Nature* **416**, 73–76.

Smith P. K. and Buseck P. R. (1981) Graphitic carbon in the Allende meteorite: a microstructural study. *Science* **212**, 322–324.

Stadermann F. J., Croat T. K., Bernatowicz T. J., Amari S., Messenger S., Walker R. M. and Zinner E. (2005) Supernova graphite in the NanoSIMS: carbon, oxygen and titanium isotopic compositions of a spherule and its TiC sub-components. *Geochim. Cosmochim. Acta* **69**, 177–188.

Stroud R. M., Chisholm M. F., Heck P. R., Alexander C. M. O'D. and Nittler L. (2011) Supernova shock-wave-induced co-formation of glassy carbon and nanodiamond. *Astrophys. J.* **738**, L27 (5pp).

Tan P., Dimovski S. and Gogotsi Y. (2004) Raman scattering of non-planar graphite: arched edges, polyhedral crystals, whiskers and cones. *Philos. Trans. R. Soc. Lond. A* **362**, 2289–2310.

Tao H., Moser J., Alzina F., Wang Q. and Sotomayor-Torres C. M. (2011) The morphology of graphene sheets treated in an ozone generator. *J. Phys. Chem. C* **115**, 18257–18260.

Timmes F. X., Woosley S. E., Hartmann D. H. and Hoffman R. D. (1996) The production of ^{44}Ti and ^{60}Co in supernovae. *Astrophys. J.* **464**, 332–341.

Thomsen C. and Reich S. (2000) Double resonant Raman scattering in graphite. *Phys. Rev. Lett.* **85**, 5214–5217.

Travaglio C., Gallino R., Amari S., Zinner E., Woosley S. and Lewis R. S. (1999) Low-density graphite grains and mixing in type II supernovae. *Astrophys. J.* **510**, 325–354.

Tuinstra F. and Koenig J. L. (1970) Raman spectrum of graphite. *J. Chem. Phys.* **53**, 1126–1130.

Wedeking K. W. and Hayes J. M. (1983) Carbonization of Precambrian kerogens. In *Advances in Geochemistry* (ed. M. Bjoroy). Wiley, Chichester, UK, pp. 546–553.

Wopenka B. (1988) Raman observations on individual interplanetary dust particles. *Earth Planet. Sci. Lett.* **88**, 221–231.

Wopenka B. (2012) Raman spectroscopic investigation of two grains from comet 81P/Wild 2: information that can be obtained beyond the presence of sp^2-bonded carbon. *Meteorit. Planet. Sci.* **47**, 565–584.

Wopenka B. and Pasteris J. D. (1993) Structural charcterization of kerogens to granulite-facies graphite: applicability of Raman spectroscopy. *Am. Mineral.* **78**, 533–557.

Wopenka B., Groopman E. and Zinner E. (2011a) Orgueil low-density presolar carbon ain't graphite but glassy carbon. *Meteorit. Planet. Sci.* **46**, A252.

Wopenka B., Jadhav M. and Zinner E. (2011b) Raman analysis of high-density presolar graphite grains from the Orgueil carbonaceous chondrite. *Lunar Planet Sci. XLII*. #1162 (abstr.).

Wopenka B., Xu Y. C., Zinner E. and Amari S. (2012) Murchison presolar graphite of different density fractions: a Raman perspective. *Meteorit. Planet. Sci*. **47**, #5067.

Xu Y. C., Amari S., Gyngard F., Zinner E. and Lin Y. (2012) Isotopic studies of presolar graphite grains from the Murchison meteorite. *Lunar Planet. Sci. XLIII*. #1094 (abstr.).

Ziegler J. F., Biersack J. P. and Ziegler M. D. (2008) *SRIM: The Stopping and Range of Ions in Matter*. SRIM Co., Chester, Maryland.

Zinner E. (2007) Presolar grains. In *Treatise on Geochemistry Update 1.02 (online update only)* (eds. H. D. Holland, K. K. Turekian and A. Davis). Elsevier Ltd., Oxford. pp. 1–33.

Zinner E., Amari S., Wopenka B. and Lewis R. S. (1995) Interstellar graphite in meteorites: isotopic compositions and structural properties of single graphite grains from Murchison. *Meteoritics* **30**, 209–226.

Zinner E., Amari S. and Jadhav M. (2006a) On the stellar sources of presolar graphite. Proceedings of the International Symposium "Nuclei in the Cosmos – IX" CERN, Geneva, June 25–30, 2006. *Proceedings of Science, PoS (NIC-IX)* 019.

Zinner E., Nittler L. R., Gallino R., Karakis A. I., Lugaro M., Straniero O. and Lattanzio J. C. (2006b) Silicon and carbon isotopic ratios in AGB stars: SiC grain data, models, and the galactic evolution of the Si isotopes. *Astrophys. J.* **650**, 350–373.

Associate editor: Anders Meibom